

Feedback in the dark: a critical examination of CMB bounds on primordial black holes

Dominic Agius,^a Rouven Essig,^b Daniele Gaggero,^c
Francesca Scarcella,^d Gregory Suczewski,^b Mauro Valli^e

^aInstituto de Fisica Corpuscular (IFIC), Universidad de Valencia-CSIC, 46071, Valencia, Spain

^bC.N. Yang Institute for Theoretical Physics, Stony Brook University, NY 11794, USA

^cINFN Sezione di Pisa, Polo Fibonacci, Largo B. Pontecorvo 3, 56127 Pisa, Italy

^dLaboratoire Univers et Particules de Montpellier (LUPM), Université de Montpellier & CNRS, 34095 Montpellier, France

^eINFN Sezione di Roma, Piazzale Aldo Moro 2, I-00185 Rome, Italy

E-mail: dominic.agius@ific.uv.es, gregory.suczewski@stonybrook.edu,
francesca.scarcella@umontpellier.fr

Abstract. If present in the early universe, primordial black holes (PBHs) will accrete matter and emit high-energy photons, altering the statistical properties of the Cosmic Microwave Background (CMB). This mechanism has been used to constrain the fraction of dark matter that is in the form of PBHs to be much smaller than unity for PBH masses well above one solar mass. Moreover, the presence of dense dark matter mini-halos around the PBHs has been used to set even more stringent constraints, as these would boost the accretion rates. In this work, we critically revisit CMB constraints on PBHs taking into account the role of the local ionization of the gas around them. We discuss how the local increase in temperature around PBHs can prevent the dark matter mini-halos from strongly enhancing the accretion process, in some cases significantly weakening previously derived CMB constraints. We explore in detail the key ingredients of the CMB bound and derive a conservative limit on the cosmological abundance of massive PBHs.

Keywords: primordial black holes, cosmic microwave background, dark matter, accretion

Contents

1	Introduction	1
2	Accretion models in the cosmological setting	4
2.1	The background cosmology	4
2.2	The Bondi–Hoyle–Lyttleton model	5
2.3	The Park-Ricotti accretion model	6
3	The role of DM mini-halos	7
3.1	Analytical modelling	8
3.2	Impact on the accretion rate: BHL and PR scenarios	9
3.3	General remarks	10
4	Constraining the PBH abundance with CMB physics	11
4.1	Energy injection from accreting matter	12
4.2	Energy deposition	13
4.3	Comparison with cosmological data	14
5	Results: The CMB bound with radiative feedback and DM mini-halos	16
5.1	The impact of the accretion model	16
5.2	The impact of DM mini-halos	18
6	Results: Assessment of the astrophysical uncertainties	18
6.1	Ionized sound speed	18
6.2	Radiative efficiency	19
6.3	Energy deposition function	19
6.4	A conservative cosmological bound	20
7	Discussion and conclusions	22
A	Details on the Park-Ricotti model	24
B	Details on the numerical analysis	25
C	Comparison to previous works	25
C.1	Comparison to Ref. [1]	26
C.2	Comparison to Ref. [2]	27

1 Introduction

The cosmic dark ages, situated between recombination and reionization, were characterized by a very low ionization fraction. During this period, the energy density of the universe was dominated by adiabatically cooling dark matter (DM) and baryons, with the latter mostly in the form of neutral hydrogen. No astrophysical processes involving copious emission of thermal or non-thermal radiation are expected to have been present in this epoch, which makes it a powerful probe of new physics that produces such radiation.

Any extra energy injection, such as particle DM annihilation or decay, can significantly heat, excite, and ionize the baryonic gas. These alterations of the baryonic medium can modify the optical depth and the visibility function of the relic photons that decoupled from the baryons shortly after recombination, ultimately affecting the anisotropies of the cosmic microwave background (CMB). This powerful way to constrain new physics was first discussed in a series of pioneering papers at the beginning of the century [3–8].

Primordial black holes (PBHs), which may constitute a component of DM, can be probed in a similar way. If massive enough, PBHs will efficiently accrete the surrounding medium, heating the baryons and emitting a broad spectrum of ionizing photons that can alter the CMB power spectrum. This idea was first discussed in [9] and later developed, for instance in [1, 2, 10–14], setting stringent upper limits on the cosmological abundance of PBHs of mass above $\mathcal{O}(10) M_{\odot}$.

However, these works relied on the classic Bondi-Hoyle-Lyttleton (BHL) model [15, 16] to quantify the rate of gas accretion onto PBHs, a central ingredient in the modelling of the energy injection into the medium.

The BHL model exists as an interpolation between two regimes: the first being the ballistic regime, considering accretion onto a point mass moving with a constant velocity through a gas of constant density and considering only gravitational effects [15], and the second being the accretion onto a spherically symmetric body at rest including the effects of pressure and gravitation [17]. It is emphasized that this interpolation formula should only be considered as an order-of-magnitude estimate of the accretion rate [2]. Moreover, given its simplified assumptions, the BHL model is unable to account for the role of radiation feedback, which is expected to play a crucial role in the physics of accretion. It is therefore compelling to move beyond the BHL formalism and to take into account the fluid and radiation effects that may significantly alter the behavior of the accretion rate as a function of the PBH speed and the properties of the medium. To this end, the Park-Ricotti model [18–20] offers a more realistic prescription for the study of accretion effects in PBHs. The authors of [18–20] performed hydrodynamic simulations of accretion onto a compact object, taking into account the effects of photo-heating and photo-ionization of the environment. These simulations captured the formation of an ionization front, in some cases preceded by a shock wave, and found a strong suppression of the accretion rate for low values of the PBH velocity. This behavior, more complex than that predicted by the classic BHL model, is well reproduced by the analytical model proposed by the authors (henceforth referred to as the PR model). The PR model can be regarded as the current state-of-the-art description of the accretion process onto isolated compact objects.

Given the expected significant departure of the accretion rate from the standard treatment, it is compelling to revisit the CMB bounds on PBHs taking into account the role of radiation feedback. This was recently done in [1], where this constraint was re-derived using the PR model. The authors showed that the bound could be relaxed by combining the PR model with conservative assumptions about the energy emission mechanism.

Irrespective of the accretion model used, PBHs are not allowed to constitute all of the DM (in the mass range where the constraint applies). Therefore, the effects of the remaining DM, whatever its nature, must be accounted for. Dense DM structures with steep density profiles are expected to build up around PBHs, starting soon after their formation. It has been argued [14, 21] that the gravitational potential produced by these mini-halos can significantly boost the accretion rate. CMB constraints on the abundance of PBHs have then been re-derived taking this into account [14], resulting in a significant strengthening of

the constraint, by up to three orders of magnitude. However, Ref. [14] relied on the BHL model to describe the accretion rate, ignoring the effect of radiation feedback. It is natural to inquire whether this strong boost on the accretion rate from DM mini-halos still occurs in the presence of a hot, ionized region around the PBH, which is known to dramatically affect the accretion process.

Motivated by these considerations, we address in the present paper for the first time the *combined impact* of two key aspects: (i) the role of the radiation feedback (as implemented in the PR model), and (ii) the impact of DM mini-halos on CMB accretion constraints on the PBH abundance. To do so, we consistently model the role of DM mini-halos within the PR model, and obtain the corrected accretion rate and the corresponding constraints on the fraction of DM in the form of PBHs, f_{PBH} . The novel constraint obtained in this way is compared in detail to the ones obtained under simpler assumptions: the BHL model in the absence of DM mini-halos, the BHL model in the presence of DM mini-halos, and the PR model in the absence of DM mini-halos.

Besides the crucial issue of the interplay between the accretion rate modeling and the presence of the DM mini-halos, it is important to recognize that other sources of uncertainty are very relevant in the problem under consideration. In particular, we will consider three additional sources of uncertainty:

- The first uncertainty is specific to the PR model, which requires a choice of sound speed within the ionized region.
- The second unknown resides in the mechanism that transforms the gravitational energy of the accreted material into heat and ionizing radiation, which eventually alters the evolution of the ionization fraction of the universe. Early works considered simplified emission models, based on the assumption that the accretion flow is spherically symmetric and thermal bremsstrahlung is the dominant radiation process. However, recent developments have highlighted the crucial role of accretion disks [2, 14]. Accretion disks are ubiquitous in the universe, and plausible arguments suggest that they can form around PBHs as early as the dark ages. The processes that are responsible for the transport of energy and angular momentum in the disk and that control the non-thermal emission of radiation are highly complex and lead to a large systematic uncertainty on the CMB bound on PBHs. In particular, the amount of energy transferred to the leptonic part of the accretion flow plays a pivotal role, since the electrons are responsible for most of the emission of the ionizing radiation (see, e.g., the discussion in [22]). A detailed assessment of the impact of this key ingredient helps determine the robustness of the CMB bound.
- The third major unknown is the actual deposition of the injected energy into the ambient medium. The energy can be deposited via three main channels, ionization, excitation, and heating, all of which are captured by the redshift-dependent energy deposition functions. Several parameterizations exist in the literature [23–25], which we will use to quantify this uncertainty.

Given this complicated tapestry of astrophysical effects, we present here a comprehensive discussion of the robustness of the CMB bound on the PBH abundance with respect to these ingredients. We systematically assess how the constraint is affected by all the elements discussed so far, and show the impact on the posterior probability distribution of f_{PBH} of the

aforementioned elements that affect the bound, with special focus on the radiative efficiency and the energy deposition function.

The rest of the paper is structured as follows. In §2, we describe the details of the accretion models considered in this work in the dark ages background cosmology. In §3, we discuss the role of DM mini-halos. In §4, we describe the key ingredients needed to calculate the CMB constraints. In §5, we present the main results of our work, illustrating the interplay between the impact of the radiation feedback and the DM mini-halos. In §6, we assess the role of astrophysical uncertainties on the CMB bound. In §7, we comment about future improvements of our analysis and present our conclusions.

2 Accretion models in the cosmological setting

The first step towards the derivation of the cosmological bound is the modelling of the rate of accretion of baryonic gas onto PBHs during the dark ages. In this epoch (the most relevant redshift range is $z \sim 100 - 1000$) structures have not yet formed. As was done in previous works [2, 14], we assume that density variations in the accreted gas are negligible and that the gas can be treated as a homogeneous medium, whose temperature and density decrease adiabatically with time according to the cosmological model. We assume that PBHs are distributed smoothly in the universe following the DM distribution. The PBH-gas velocity is then expected to trace the cosmological baryon-DM velocity. We assume that the energy injection can be considered spatially homogeneous. This picture is expected to break down at later times, when virialized halos start to form, but is typically considered reliable in the redshift range that is relevant for the CMB bound. We mention in the final discussion possible caveats associated with these assumptions, related to the early formation of structures in Λ PBH cosmologies. Finally, we assume that PBHs are characterized by a monochromatic mass distribution.¹

In this section, we first review the background cosmology that describes the evolution of the baryonic medium and the DM component with redshift, based on which we model the accreted gas and the PBHs. We then review the classic BHL model before summarizing the main aspects of the PR model, on which we rely to account for the role of radiative feedback.

2.1 The background cosmology

The background cosmological density of baryons ρ_b scales as

$$\rho_b = \rho_{b,\text{rec}} \frac{(1+z)^3}{(1+z_{\text{rec}})^3}, \quad (2.1)$$

where the baryon density at recombination is $\rho_{b,\text{rec}} \simeq 200 \text{ cm}^{-3}$ and the redshift of recombination is $z_{\text{rec}} \sim 1100$. The sound speed of the baryons c_s depends on the background temperature T and on the ionization fraction X_e , such that

$$c_s = \sqrt{\frac{\gamma(1+X_e)T}{m_p}} \text{ km s}^{-1}, \quad (2.2)$$

¹Extended mass functions, as predicted by simple single-field inflationary scenarios, have been shown to typically tighten the CMB bounds on PBH abundance [2, 26–28]. We will comment on this further in §7.

where m_p is the proton mass and γ is the adiabatic index. We take the average velocity between PBHs and the background gas v_{rel} to be equal to the linear cosmological baryon-DM relative speed [29, 30], which is given by

$$\sqrt{\langle v_{\text{rel}}^2 \rangle} = \min \left[1, \frac{1+z}{1000} \right] \cdot 30 \text{ km s}^{-1} . \quad (2.3)$$

The PBH velocity distribution is assumed to be described by a Maxwell–Boltzmann distribution centered around this mean value.

2.2 The Bondi–Hoyle–Lyttleton model

According to the BHL accretion model [15, 17], the accretion rate onto an isolated compact object, characterized by its mass M and speed v_{rel} , is given by

$$\dot{M}_{\text{BHL}} = 4\pi\lambda \frac{(GM)^2 \rho_b}{(v_{\text{rel}}^2 + c_s^2)^{3/2}} , \quad (2.4)$$

where ρ_b and c_s are the ambient medium density and sound speed, respectively, and λ is a constant suppression factor (see below). The BHL accretion rate can also be expressed in terms of an effective cross section

$$\dot{M}_{\text{BHL}} = 4\pi\lambda\rho_b \frac{G^2 M^2}{v_{\text{eff}}^3} = 4\pi\lambda\rho_b v_{\text{eff}} r_B^2 , \quad (2.5)$$

where the effective velocity is $v_{\text{eff}} = \sqrt{c_s^2 + v_{\text{rel}}^2}$ and r_B is the generalized Bondi radius

$$r_B = \frac{GM}{v_{\text{eff}}^2} . \quad (2.6)$$

In several works, both in astronomical and cosmological settings, the BHL formula is corrected ad-hoc by a suppression factor λ . In the astronomical context, a value of $\lambda \sim 10^{-2} - 10^{-3}$ is included to match observations of the luminous emission from accreting compact objects, such as the non-observation of a large population of isolated neutron stars [31] or astrophysical BHs [32] in the local region, as well as the studies of nearby active galactic nuclei [33], and of the supermassive BH at the Milky-Way center [34]. This factor aims to phenomenologically capture the impact of a variety of non-gravitational forces (pressure, fluid viscosity, radiation feedback, etc.), which may partially counteract the gravitational pull of the compact object and suppress the accretion rate.

Similarly, in the cosmological context, the correction to the Bondi formula due to the coupling of the gas to the CMB photon fluid (accounting for Hubble expansion and DM over-densities) has been computed and explicitly expressed as a function of several thermodynamic quantities that characterize the ambient medium [10, 13, 35]. These papers assume spherical symmetry for the accretion process and bremsstrahlung (free-free) radiation near the Schwarzschild radius as the dominant cooling process.

In the following, we use as a benchmark scenario $\lambda = 0.01$ in the context of disk accretion. However, for the spherical accretion case, which leads to weaker bounds and can be considered a conservative scenario, we will instead use the results of [13] to set the suppression factor λ .

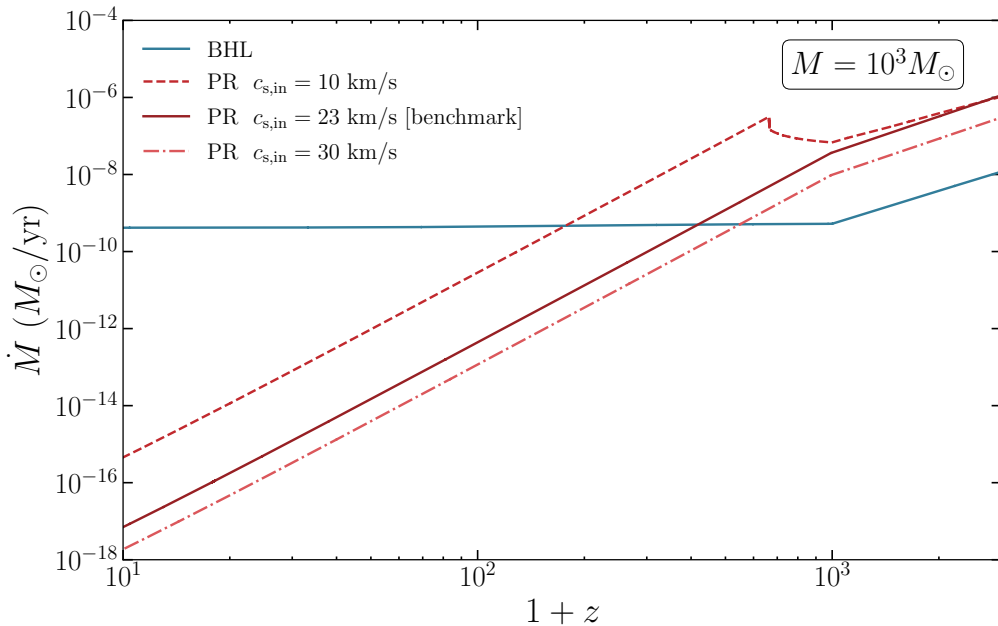


Figure 1: Accretion rate as a function of redshift for the BHL model (blue) and the PR model (red) for a $10^3 M_\odot$ PBH, assuming the setup described in §2.1. For the PR model, three different values are shown for the sound speed within the ionized region $c_{s,\text{in}}$. The Λ CDM parameters used for this plot, as well as plots below where a fixed cosmology is implied, are given by: $\{\Omega_b, \Omega_c, H_0, \ln 10^{10} A_s, n_s, z_{\text{reio}}\} = \{0.02231, 0.1198, 67.90, 3.043, 0.9674, 7.4\}$. For this plot we set $f_{\text{PBH}} = 10^{-15}$ to remove feedback effects on the background cosmology.

2.3 The Park-Ricotti accretion model

The impact of *radiative feedback* on the accretion process was studied by Park and Ricotti through hydro-dynamical simulations of accretion of a homogeneous medium into a compact object [18–20]. The simulations showed the formation of an ionization front, in some velocity regimes preceded by a shock wave, and simultaneously a sharp reduction of the accretion rate. The authors were able to reproduce the accretion rates obtained in the simulations via a simple analytical model, the PR model, which we briefly describe here.

The high-energy radiation emitted in the accretion process ionizes the gas surrounding it. Its temperature and density are affected, as well as the velocity with which it flows around the BH. This variation in the properties of the gas in turn is expected to affect the accretion rate. The PR model assumes that the BHL accretion formula, Eq. (2.4), is valid within the ionized region

$$\dot{M}_{\text{PR}} = 4\pi \frac{(GM)^2 \rho_{\text{in}}}{(v_{\text{in}}^2 + c_{s,\text{in}}^2)^{3/2}} \ , \quad (2.7)$$

where $\rho_{\text{in}}, v_{\text{in}}, c_{s,\text{in}}$ are, respectively, the density, relative velocity, and sound speed characterizing the ionized gas. The sound speed $c_{s,\text{in}}$ is set to a constant value, with $c_{s,\text{in}} \gg c_s$. The density ρ_{in} and relative speed v_{in} are obtained from the corresponding quantities ρ_b and v_{rel} , by imposing the one-dimensional conservation of mass and the equilibrium of forces across the ionization front (we assume an ideal gas and that the process is isothermal [20, 36])

$$\rho_{\text{in}} v_{\text{in}} = \rho_{\text{b}} v_{\text{rel}}, \quad (2.8)$$

$$\rho_{\text{in}}(v_{\text{in}}^2 + c_{\text{s,in}}^2) = \rho_{\text{b}}(v_{\text{rel}}^2 + c_{\text{s}}^2). \quad (2.9)$$

This system of equations admits two solutions. These describe a D-type (dense type) ionization front, which forms at low velocities ($v_{\text{rel}} < v_{\text{D}} \approx c_{\text{s}}^2/2c_{\text{s,in}}$) and an R-type front (rarefied type), which forms at high velocities ($v_{\text{rel}} > v_{\text{R}} \approx 2c_{\text{s,in}}$) (the definitions of v_{D} and v_{R} are given in [Appendix A](#)). In the intermediate velocity range, neither applies. Instead, as v_{in} reaches the speed of sound $c_{\text{s,in}}$, a shock front forms in front of the ionized region. The relative velocity v_{in} remains fixed to approximately the speed of sound $c_{\text{s,in}}$, while the gas density ρ_{in} increases with the outer velocity v_{rel} according to Eq. (2.9) (Eq. (2.8) no longer holds in the presence of the shock front). The explicit expression for the PR accretion rate is also given in [Appendix A](#).

In the high-velocity regime, $v_{\text{rel}} \gg c_{\text{s,in}}$, the BHL and PR models converge, as the ram pressure of the ambient gas dominates over the ionization pressure. In practice, however, the BHL model is multiplied by the fudge factor λ and hence predicts accretion rates that are lower by a factor λ . The PR accretion rate deviates significantly from BHL for velocities lower than v_{R} , when the shock front is formed. While the BHL rate increases sharply towards lower speeds, the PR rate decreases. In this regime, the PR rate is strongly suppressed with respect to the BHL rate.

The sound speed $c_{\text{s,in}}$ of the ionized gas, or equivalently its temperature, determines the value of v_{R} and hence the peak of the PR accretion rate. Its value is in principle determined by the balance between heating and cooling processes within the gas. In the PR model, it is treated as a free parameter. We consider as a benchmark value $c_{\text{s,in}} = 23$ km/s, corresponding to a temperature of 4×10^4 K [20]. In §6.1, we provide a detailed discussion on how the choice of $c_{\text{s,in}}$ affects the CMB bounds.

The BHL and PR accretion rates are shown as a function of redshift in [Figure 1](#), for the setup described in §2.1 and for a few different values of $c_{\text{s,in}}$ in the PR case. The plot clearly shows the effect of the radiation feedback on the accretion rate of a PBH population during the Dark Ages and naturally motivates a careful study of the impact of different choices of $c_{\text{s,in}}$ on the CMB bound. In particular, lower values of $c_{\text{s,in}}$ lead to higher accretion rates for the range of velocities relevant to our work (see [Appendix A](#)). The change in the behavior for low $c_{\text{s,in}}$ in the PR case that appears at high redshift reflects the functional dependence of \dot{M} on the PBH velocity.

3 The role of DM mini-halos

If PBHs constitute only a subdominant fraction of the DM, we expect the remainder of the DM to form dense compact mini-halos around them [21, 37–40]. These are formed in the radiation era soon after the PBHs themselves, as the DM particles decouple from the Hubble flow under the PBH’s gravitational attraction. The turnaround radius $r_{\text{t.a.}}$ for a DM particle that decouples at time $t_{\text{t.a.}}$ is well approximated by $r_{\text{t.a.}}^3 \simeq 2GMt_{\text{t.a.}}^2$ [41]. In the radiation era $t \propto a^2$, so this process leads to the formation of a density spike with a steep profile, $\rho \propto r^{-\alpha}$, with $\alpha = -9/4$. After equality, the halo keeps growing by self-similar secondary infall, expected to lead to the same radial dependence [42, 43]. The subsequent dynamical evolution of the DM particles in the spike can alter the profile [43–45], but the simple $\alpha = 9/4$

power-law remains nevertheless a good description for the range of PBH masses we consider. This profile has also been confirmed by numerical simulations [14, 41]. The DM mini-halos create an additional gravitational potential around the BH, which is expected to boost the accretion rate [14, 21]. In particular, it was shown in Ref. [14] that DM mini-halos can have a dramatic impact on the CMB bound on f_{PBH} , making it stronger by orders of magnitude. That analysis was carried out assuming BHL accretion; in this work, we will extend this modeling to assess the role of DM mini-halos in the context of the PR model.

3.1 Analytical modelling

As discussed in §2.3, the PR model is based on the description of a BHL accretion problem taking place within an ionized region around the BH. This consideration allows us to apply a similar treatment for the inclusion of DM mini-halos to that employed in [14, 46] for BHL. This consists in replacing the Bondi radius r_{B} in Eq. (2.6) with an effective radius $r_{\text{B}}^{\text{eff}}$, which accounts for the gravitational pull of the DM halo. We write the accretion rate as

$$\dot{M} = 4\pi\rho_{\text{b}}v_{\text{eff}}(r_{\text{B}}^{\text{eff}})^2. \quad (3.1)$$

For the BHL model, $v_{\text{eff}}^{\text{BHL}} = (c_{\text{s}}^2 + v_{\text{rel}}^2)^{1/2}$. In the case of the PR model, the relevant effective velocity must be defined within the ionized region, hence we set $v_{\text{eff}}^{\text{PR}} = (c_{\text{s, in}}^2 + v_{\text{in}}^2)^{1/2}$. Given an effective velocity, the effective Bondi radius $r_{\text{B}}^{\text{eff}}$ is the radius that satisfies the following equation

$$v_{\text{eff}}^2 = \frac{GM}{r} - \phi_{\text{h}}(r), \quad (3.2)$$

where $\phi_{\text{h}}(r)$ is the gravitational potential generated by the DM mini-halos. In the PR case, this approach is self-consistent as long the effective radius obtained in this way does not exceed the size of the ionized region. We verify that this is true for the parameters relevant to this work, assuming, as estimated in [47], that the size of the ionized region is around 10^2 times larger than the Bondi radius computed within the ionized region.

The square root of the right-hand side of Eq. (3.2) represents an escape velocity, which depends on r . For $r < r_{\text{B}}^{\text{eff}}$, this velocity is larger than the effective velocity v_{eff} that characterizes the gas, and the gas can be captured and accreted by the PBH. Conversely, when v_{eff} is larger than this quantity, due to either a large sound speed or large flow velocity of the gas around the PBH, the gas is able to escape the gravitational field of the PBH.

We model the DM mini-halos with a power law density profile $\rho_{\text{h}}(r)$ and a sharp cutoff at the halo radius $r = r_{\text{h}}$

$$\rho_{\text{h}}(r) = \rho_{\text{h},0} \left(\frac{r}{r_{\text{h}}} \right)^{-\alpha}, \quad r < r_{\text{h}}. \quad (3.3)$$

Motivated by the discussion at the beginning of this section, we set the power law index to $\alpha = 9/4$. The halo radius and the normalization constant depend on the PBH mass and evolve with redshift. Adopting the same model as the one employed in [14], we set the total halo mass M_{h} and halo radius r_{h} respectively to

$$\begin{aligned} M_{\text{h}} &\simeq \frac{3000}{1+z} M, \\ r_{\text{h}} &\simeq 58 \text{ pc } (1+z)^{-1} \left(\frac{M_{\text{h}}}{M_{\odot}} \right)^{1/3}. \end{aligned} \quad (3.4)$$

The gravitational potential generated by the DM mini-halos is then given by

$$\phi_h(r) = \begin{cases} \frac{GM_h}{\alpha - 2} \left(\frac{3 - \alpha}{r_h} - \frac{r^{2-\alpha}}{r_h^{3-\alpha}} \right), & r < r_h, \\ -\frac{GM_h}{r}, & r \geq r_h. \end{cases} \quad (3.5)$$

Combining Eqs. (3.2) – (3.5), we obtain an equation for the effective Bondi radius for a given value of the effective velocity

$$v_{\text{eff}}^2 = \begin{cases} \frac{GM}{r_{\text{B}}^{\text{eff}}} + \frac{GM_h}{(\alpha - 2) r_{\text{B}}^{\text{eff}}} \left[\left(\frac{r_{\text{B}}^{\text{eff}}}{r_h} \right)^{3-\alpha} - (3 - \alpha) \frac{r_{\text{B}}^{\text{eff}}}{r_h} \right], & r_{\text{B}}^{\text{eff}} < r_h, \\ \frac{GM}{r_{\text{B}}^{\text{eff}}} + \frac{GM_h}{r_{\text{B}}^{\text{eff}}}, & r_{\text{B}}^{\text{eff}} \geq r_h. \end{cases} \quad (3.6)$$

From here we can obtain the effective Bondi radius for the BHL and PR cases, setting $v_{\text{eff}} = v_{\text{eff}}^{\text{BHL}}$ and $v_{\text{eff}} = v_{\text{eff}}^{\text{PR}}$, respectively. We solve Eq. (3.6) numerically for both models. Having obtained the effective Bondi radius, we compute the enhanced accretion rate through Eq. (3.1).

3.2 Impact on the accretion rate: BHL and PR scenarios

In the BHL case, we find that the effective Bondi radius increases significantly towards low redshifts, becoming larger than the Bondi radius in the absence of DM mini-halos by orders of magnitude. In contrast, we find that when the PR model is considered, only a slight increase in the effective radius occurs, and only for large PBH masses. In most cases, the growth is negligible.

The reason for this strikingly different behavior is illustrated in Figure 2. We show the evolution with redshift of the total potential $-\phi_{\text{tot}} = -\phi_{\text{BH}} - \phi_h$, with $\phi_{\text{BH}} = -GM/r$, and of the effective velocity v_{eff} . The effective Bondi radius is given by the intersection between these curves, according to Eq. (3.2).

Two factors contribute to the increase of the effective Bondi radius towards low redshifts: on the one hand, the increasing volume of the DM spike; on the other hand, the decreasing value of the effective velocity. As the DM potential builds up in the outskirts, the central region ($r \lesssim 1$ pc, depending on the PBH mass) remains dominated by the gravitational field of the PBH. At early times, high temperatures and large baryon gas-DM relative velocities v_{rel} (see §2.1) both contribute to a high v_{eff} . Consequently, only the central PBH-dominated region is involved in the accretion process. At later times, the temperature decreases, and the relative velocity is redshifted. In the BHL case, this implies a decreasing v_{eff} , and the inclusion of a progressively larger portion of the DM-halo within the radius relevant for accretion. Especially for large masses, the contribution of the halo to the gravitational potential eventually comes to dominate the accretion process, as the effective Bondi radius extends beyond the size of the DM mini-halo.

Figure 3 shows the ratio between the accretion rates with and without DM mini-halos. In the case of BHL accretion (left panel), the effect is dramatic, especially at low redshifts: the accretion rate is boosted by up to five orders of magnitude. The transition between two regimes, a PBH-dominated regime at high redshift and a halo-dominated regime at low redshift, can be clearly appreciated in the figure: at low redshifts, the DM-halo is entirely

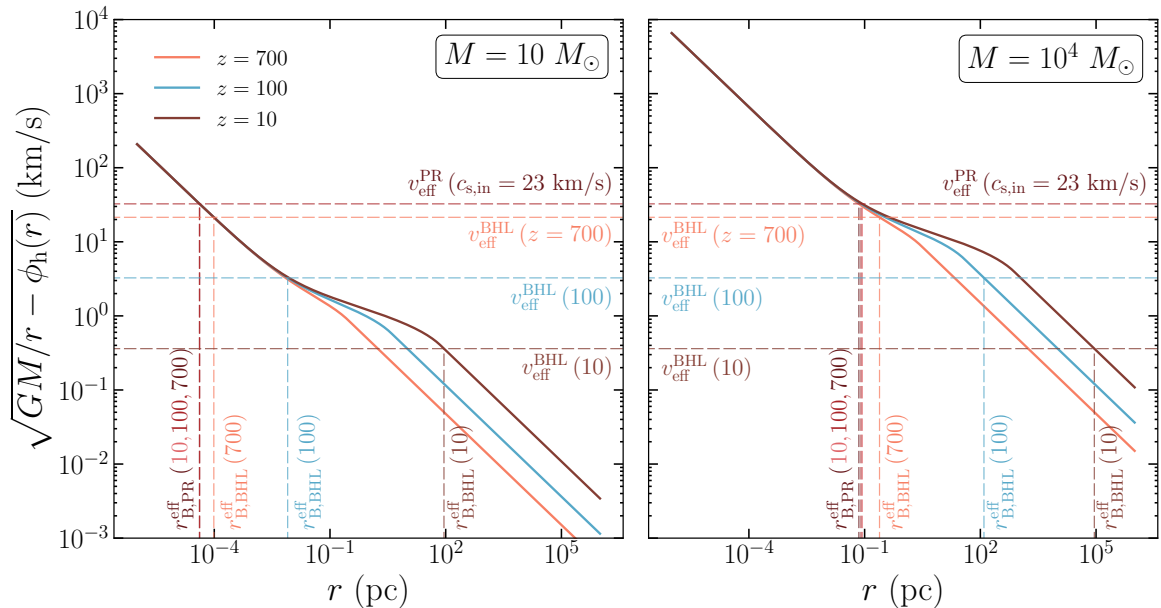


Figure 2: Graphical representation of the right-hand-side of Eq. (3.2). The solid lines trace the sum of the total (PBH plus DM mini-halo) potential at different redshifts. The horizontal lines show the values of the effective velocity v_{eff} within the physical setup described in §2.1, for a fixed Λ CDM cosmology with $f_{\text{PBH}} = 10^{-15}$. For the BHL model, v_{eff} varies with z . Within the PR model, it remains almost constant. The intersection between the horizontal lines and the curves describing the potential determines the value of the effective Bondi radius $r_{\text{B}}^{\text{eff}}(z)$, denoted here by $r_{\text{eff}}^{\text{BHL}}$ and $r_{\text{eff}}^{\text{PR}}$ for the BHL and PR models, respectively.

enclosed by the effective Bondi radius, and the increase of the accretion rate is driven by its growth.

The picture changes in the PR scenario. In this case, the relevant effective velocity is determined by the temperature and velocity of the gas *within the ionized region* surrounding the BH. The much higher temperature of the ionized gas maintains v_{eff} high. Furthermore, the relative velocity of the ionized medium with respect to the PBH remains constant (in the intermediate velocity regime, the gas velocity is set to by $v_{\text{in}} = c_{\text{s,in}}$). Consequently, v_{eff} does not decrease with time. The only factor contributing to the variation of the Bondi radius is the growth of the DM halo. However, as shown in Figure 2, the high value of v_{eff} significantly restricts the region relevant for accretion. The central part of the potential is dominated by the PBH potential, and hence the DM spike build-up has a negligible effect (a small variation in $r_{\text{B}}^{\text{eff}}$ due to the growth of the halo can be appreciated for $M_{\text{BH}} = 10^4 M_{\odot}$ at $z \sim 10$).

The right panel of Figure 3 shows that, when the PR model is considered, the ratio between the accretion rates remains of order one for all redshifts: the high effective velocity prevents the DM mini-halo from contributing significantly to the accretion process.

3.3 General remarks

While we have obtained this result in the context of a specific model, our analysis leads us to a more general conclusion. We recognize that the high temperature (sound speed) of the local gas is a sufficient condition for the DM mini-halos to play a marginal role in the accretion process. For typical values of the ionized gas temperature, $T \sim \mathcal{O}(10^4)$, accretion

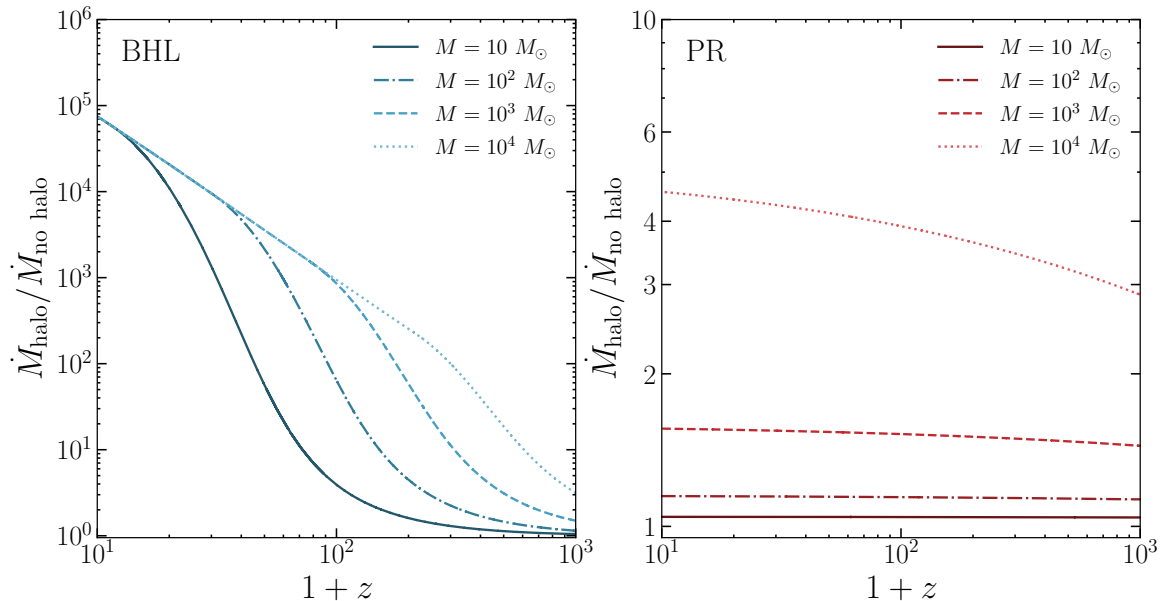


Figure 3: Ratio between the accretion rates with and without DM mini-halos around the PBH, for the BHL (left) and PR (right) models. Here we assume the same fixed cosmology as described in the caption of Figure 1.

is mostly confined to the volume dominated by the PBH potential, and the ratio between the accretion rate with and without DM mini-halos is never larger than a factor of a few (for the values of the PBH mass considered here). This result has an intuitive interpretation: the high velocity dispersion of the heated gas particles reduces the effective cross section for the accretion process. This process remains confined to a small volume around the PBH, where the gravitational field is dominated by the PBH potential.

While the PR model provides a simple prescription to account for the local increase in temperature around the PBH, this is expected to occur in general, as a consequence of the accretion of gas and corresponding energy release. The energy injection is necessarily bound to have some degree of locality and hence to cause the local effective velocity to rise. This discussion suggests that CMB constraints presented in the literature, which to the best of our knowledge did not take this into account, may have significantly overestimated the impact of DM mini-halos on the bound.

4 Constraining the PBH abundance with CMB physics

In this section, we describe in detail how the accretion of gas onto PBHs is expected to modify the anisotropies of the CMB, and how we can use this observable to constrain the PBH abundance. In particular, we discuss the phenomena governing the emission of radiation from the accreting gas and its deposition into the plasma, as well as the associated modelling uncertainties. We discuss the impact of this energy injection on the hydrogen ionization fraction and on the observed CMB temperature power spectrum. Finally, we present some details of our statistical analysis.

4.1 Energy injection from accreting matter

The total energy injection into the medium per unit volume is given by

$$\left. \frac{d^2 E}{dV dt} \right|_{\text{inj}} = L n_{\text{PBH}} = L f_{\text{PBH}} \frac{\rho_{\text{DM}}}{M}, \quad (4.1)$$

where L is the bolometric accretion luminosity of a PBH of mass M , which is a function of the accretion rate \dot{M} . Accretion is a very powerful energy converter. The bolometric luminosity is related to the total influx of rest-mass energy of the accreted material via the ϵ parameter that measures the *radiative efficiency*:

$$L = \epsilon \dot{M} c^2. \quad (4.2)$$

Here, ϵ is, in general, a function of \dot{M} , and typically takes the functional form of a power law $\epsilon(\dot{M}) \propto \dot{M}^a$, where a and the normalization can vary significantly depending on whether or not an accretion disk is formed, and on the type of accretion disk.

The basic criterion used to assess whether an accretion disk can form is to estimate the angular momentum of the baryons: if it is large enough to keep the gas in Keplerian rotation well beyond the innermost stable orbit, then a disk can form [48]. Following [2], the condition for disk formation can be written as

$$f_{\text{PBH}} \frac{M}{M_{\odot}} \ll \left(\frac{1+z}{730} \right)^3. \quad (4.3)$$

We make the assumption that a disk *always* forms.² We relax this assumption in §6.4 to derive a conservative bound.

The complex processes that shape the transport of energy and angular momentum in the disk and the associated non-thermal emission represent an important source of uncertainty when assessing the CMB bound. In accretion disks, the angular momentum of the rotating matter is gradually transported outwards by stresses (related to turbulence, viscosity, shear, and magnetic fields), and matter flows inwards. Energy is typically transferred to the electrons, which are responsible for the non-thermal cooling via synchrotron, bremsstrahlung, and inverse Compton, and is ultimately radiated away. The accretion scenario that we are considering is characterized by low values of the accretion rate, well below the Eddington value. In this situation, the accretion flow is typically not dense enough to guarantee efficient coupling between ions and electrons, as is instead the case for *thin disks* [49]. Hence, the dissipated energy is not efficiently radiated away by the leptonic component and is advected into the central black hole. The accretion disk that corresponds to this scenario is hot and geometrically thick, and is usually called *Advection-Dominated Accretion Flow* (ADAF). The ϵ parameter in the ADAF model is linearly suppressed for smaller accretion rates.

The physics behind the suppression of the radiative efficiency is typically captured by a parameter called δ , which quantifies the fraction of turbulent energy that heats the electrons directly. Magneto-hydro-dynamic (MHD) turbulence is the main physical process ultimately responsible for the transfer of energy and angular momentum in the accretion flow: turbulent energy is dissipated at small scales via kinetic damping mechanisms that generally transfer

²We have verified *a posteriori* that this is mostly the case for the range of PBH masses considered in this work for allowed values of f_{PBH} (including those ruled out by non-CMB bounds as shown in Figure 6) and in the redshift range that has the most constraining power, i.e., typically $z \sim \mathcal{O}(100 - 1000)$.

δ	$\dot{M}_{\text{net}} / \dot{M}_{\text{Edd}}$ Range	ϵ_0	a
0.5	$< 2.9 \times 10^{-5}$	1.58	0.65
	$2.9 \times 10^{-5} - 3.3 \times 10^{-3}$	0.055	0.076
	$3.3 \times 10^{-3} - 5.3 \times 10^{-3}$	0.17	1.12
0.1 [benchmark]	$< 9.4 \times 10^{-5}$	0.12	0.59
	$9.4 \times 10^{-5} - 5.0 \times 10^{-3}$	0.026	0.27
	$5.0 \times 10^{-3} - 6.6 \times 10^{-3}$	0.50	4.53
10^{-3}	$< 7.6 \times 10^{-5}$	0.065	0.71
	$7.6 \times 10^{-5} - 4.5 \times 10^{-3}$	0.020	0.47
	$4.5 \times 10^{-3} - 7.1 \times 10^{-3}$	0.26	3.67

Table 1: The piecewise power-law fitting formulae giving the radiative efficiency parameters needed to compute Eq. (4.4), taken from [22].

energy to the ions and electrons at different rates, with a preference to the heavy component. Hence, this parameter was initially believed to be very small, $\mathcal{O}(10^{-3})$ in early works on ADAF modeling. However, further investigation has demonstrated that the electrons can indeed receive a comparable fraction of turbulent heating to that of the ions due to a variety of mechanisms including magnetic reconnection [50–52]. In this work we do not aim at modeling the complex physics that shapes these processes. Instead, we follow the approach of [22]: we bracket the associated uncertainties by treating δ as a free parameter. For different reference values of δ , the authors solve a set of equations that describe a two-fluid ADAF and compute both its dynamical structure (temperature and density profile) and the non-thermal emission.

The main output of these calculations is to define the behavior of the radiative efficiency ϵ as a function of the accretion rate \dot{M} , which has the functional form

$$\epsilon(\dot{M}) = \epsilon_0 \left(\frac{\dot{M}}{0.01\dot{M}_{\text{edd}}} \right)^a, \quad (4.4)$$

where \dot{M}_{edd} is the Eddington accretion rate. The parameters ϵ_0 and a characterizing the model take a piecewise functional form explicitly dependent on the accretion rate, and are defined in table I of [22]. For typical values of the accretion rate in the PR model, using the benchmark of $\delta = 0.1$, we have $\epsilon_0 = 0.12$ and $a = 0.59$; this possibility, as well as the other values that we consider in this paper are detailed in Table 1. The function in Eq. (4.4) captures all the information that is needed for the problem of energy injection into the inter-galactic medium (IGM) that is of interest for our current work. We remark that our benchmark choice implies a larger radiative efficiency compared to the (very conservative) scenario of spherical accretion (as investigated by [13]). On the other hand, it features a lower efficiency compared to the thin-disk case, which predicts a constant value of $\epsilon \simeq 0.1$ [49].

4.2 Energy deposition

It has been shown that energy injections during the dark ages are not necessarily deposited into the medium *on the spot*,³ and rather can be deposited at later times. The energy deposition functions, $f_c(z, X_e)$, quantify the amount of injected energy that is deposited at

³On-the-spot refers to energy being absorbed by the medium at the same redshift as it was emitted.

redshift z for a channel c , where the most relevant channels are the heating, ionization, and excitation of atoms. Equivalently, $f_c(z, X_e)$ can be decomposed into an injection efficiency function $f_{\text{eff}}(z)$, and a deposition fraction $\chi_c(z, X_e)$. These recipes for computing the redshift dependence of energy injection and deposition are quantified through the relation

$$\left. \frac{d^2 E}{dV dt} \right|_{\text{dep},c} = f_c(z, X_e) \left. \frac{d^2 E}{dV dt} \right|_{\text{inj}} = f_{\text{eff}}(z) \chi_c(z, X_e) \left. \frac{d^2 E}{dV dt} \right|_{\text{inj}}, \quad (4.5)$$

where the first equality makes use of the energy deposition functions, f_c , and the second uses the deposition fractions, χ_c . Both methodologies are equivalent at the level of Eq. (4.5). However, they correspond to two different approaches for computing the energy deposition that have been adopted in the recent literature [24, 53]. We quantify the effect of these two approaches on the bound in §6.

- The *energy deposition fraction* prescription has been recently used to compute CMB bounds for PBHs using PR accretion [1], where the authors used the $f_{\text{eff}}(z)$ computed analytically in [13] combined with the deposition fractions tabulated from [53]. We refer to this as the analytic case.
- Alternatively, authors have also recently used the *energy deposition function* prescription, where the energy deposition functions $f_c(z)$ are calculated for a given energy-differential luminosity spectrum L_ω , using the following expression:

$$f_c(z, X_e) = H(z) \frac{\int \frac{d \ln(1+z')}{H(z')} \int T(z', z, \omega) L_\omega d\omega}{\int L_\omega d\omega}, \quad (4.6)$$

where L_ω is the energy-differential luminosity spectrum, and the transfer functions $T(z', z, \omega)$ are tabulated from [23, 24]. These transfer functions are computed numerically down to energies of 5 keV, however, some authors have suggested that they can be extrapolated down to 100 eV, and thus set the lower bound in the integrals in Eq. (4.6) to this value [2, 14]. We refer to this as the extrapolated case. Rather than extrapolating it down to 100 eV, we cut the integration at the lower bound of their calculated value (5 keV), and we refer to this as the benchmark case. This prescription is the default setting in the numerical `DarkAges` script [54], which we use to perform the integral in Eq. (4.6). Note that one of the key assumptions in the calculation of the transfer functions using this prescription is that the altered free electron fraction does not have a feedback effect on the energy cascade evolution [54]. Recently, a new tool, `DarkHistory` [55], has been developed to self-consistently take into account this feedback effect and compute X_e -dependent transfer functions. We have chosen not to include this in our setup, as we expect the impact on the bound to be negligible.⁴

4.3 Comparison with cosmological data

Once the energy deposition formalism is set, the last step consists of computing the impact of the extra energy that is injected into the medium on the ionization fraction X_e and the IGM temperature T , and the subsequent alteration of the CMB power spectrum. The physical

⁴We compared the computed free electron fraction at the bound (i.e. $f_{\text{PBH}} 10^{-3}$ at $M = 10^3 M_\odot$ in Figure 4) to Figure 3 of [56], and verified that the impact on the computed ionization fractions between the `DarkAges` and `DarkHistory` treatments is negligible.

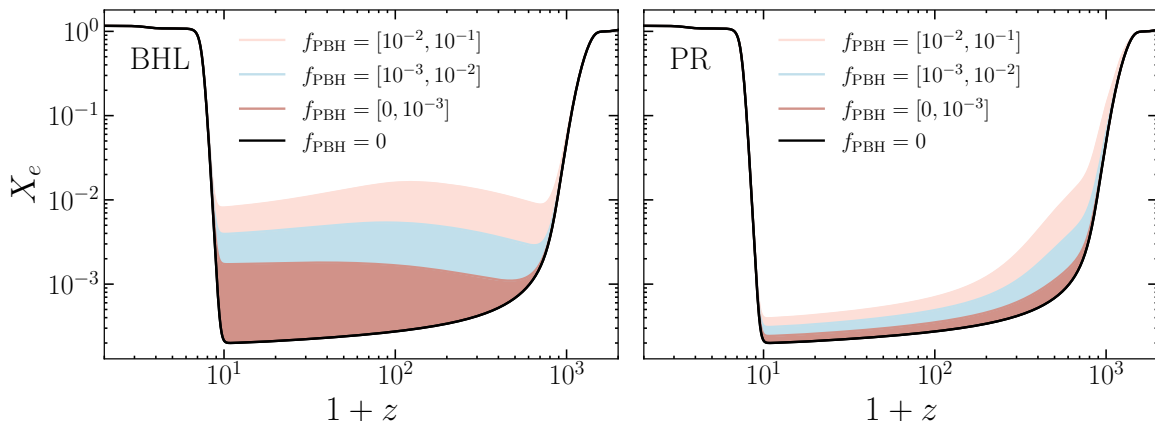


Figure 4: The free electron fraction, X_e , as a function of redshift, showing the effect of a monochromatic PBH population with mass $M_{\text{PBH}} = 10^3 M_\odot$, for different PBH abundances, as labelled. The left figure is for the BHL accretion scenario, and the right figure shows the PR scenario, with $c_{s,\text{in}} = 23$ km/s. The standard scenario Λ CDM cosmology (with parameters described in the caption of Figure 1) is described by the solid black line.

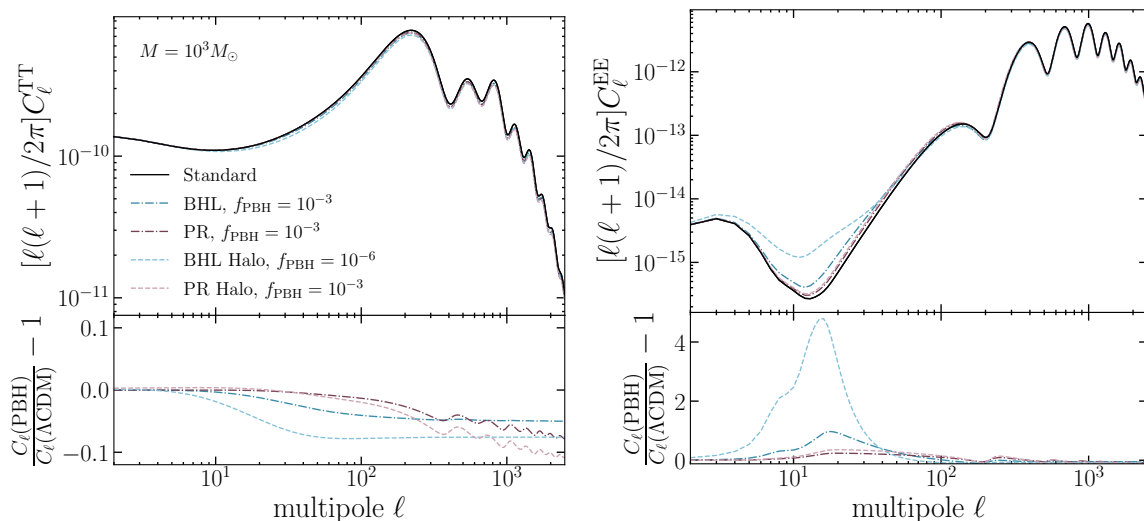


Figure 5: The impact of the accretion recipe on the CMB TT (left) and EE (right) power spectrum for a monochromatic population of PBHs with masses $M = 10^3 M_\odot$, assuming the fixed Λ CDM cosmology described in the caption of Figure 1.

processes responsible for such alterations are discussed in detail for instance in [3, 13]. The key point is the broadening of the visibility function towards lower redshift, which mainly implies a suppression of the secondary peaks due to an increase in the time available for the dissipation of acoustic oscillations [57].

To compute the CMB and large scale structure observables corresponding to the simulated evolution of linear perturbations from the early universe, we use the latest version of the publicly available Boltzmann solver CLASS [58]. In particular, we implement modifications to CLASS, altering the thermal history of the universe to include the effect of accreting PBHs. We base our approach on the framework presented in ExoCLASS [54], making modifications to

Model	$c_{s,\text{in}}$	λ	δ	Energy deposition treatment
BHL	n/a	0.01	0.1	$f_c(z)$ computed using Eq. (4.6) with details in §4.2
PR	23 km/s	n/a	0.1	$f_c(z)$ computed using Eq. (4.6) with details in §4.2

Table 2: The benchmark values of the main parameters under consideration, with full descriptions of each parameter provided in §4. In §6, we show the impact on the bound when varying $c_{s,\text{in}}$ for the PR model, the parameter δ , and the energy deposition treatment.

include our recipes. For illustrative purposes, we show in Figure 4 and Figure 5 the impact of the addition of a population of radiating PBHs for different values of f_{PBH} .

This modified version of CLASS is then interfaced with the Bayesian analysis code Cobaya [59, 60], to perform a Markov Chain Monte Carlo (MCMC) simulation to probe the 7-dimensional $\Lambda\text{CDM} + f_{\text{PBH}}$ parameter space,

$$\Lambda\text{CDM} + f_{\text{PBH}} \equiv \{\Omega_b, \Omega_c, H_0, A_s, n_s, z_{\text{reio}}\} + f_{\text{PBH}}, \quad (4.7)$$

where 9 masses evenly log-spaced in the range of $M_{\text{PBH}} \in [10^1, 10^4] M_\odot$ are probed. These parameters are constrained using the latest state-of-the-art likelihoods from Planck, SPT, ACT and BAO. We use flat priors for each of the cosmological parameters, described in detail in Appendix B. In particular, we constrain the cosmological parameters (4.7) using *Planck* 2018 high- l TTTEEE, low- l TT, low- l EE [61]; the isotropic BAO measurements from 6dFGS at $z_{\text{eff}} = 0.106$ [62] and from the Sloan Digital Sky Survey Data Release 7 at $z_{\text{eff}} = 0.15$ [63]; the anisotropic BAO and growth function $f\sigma_8(z)$ measurements made using the CMASS and LOWZ galaxy samples of BOSS DR12 [64] and DR16 [65]; 2022 SPT 3g TTTEEE [66]; ACT DR4 [67, 68] and ACT DR6 + Planck2018 lensing [69–71]. We consider runs to be converged with the Gelman-Rubin criterion, when $|R - 1| < 0.05$ [72]. The bound is computed as the 95% probability using a highest-density interval calculation [73].

5 Results: The CMB bound with radiative feedback and DM mini-halos

We now consider the benchmark values of the main free parameters under consideration (given in Table 2), and assess the impact on the bound of the accretion model and of the inclusion of DM mini-halos. The updated CMB bound on the abundance of PBHs, according to the assumption and the data described in the previous sections, are displayed in Figure 6 for a few selected reference scenarios: (i) Bondi-Hoyle-Lyttleton accretion in absence of a relevant contribution of dark-matter mini halos, with the fudge factor set to $\lambda = 0.01$; (ii) Park-Ricotti accretion in absence of DM mini-halos; (iii) BHL accretion with DM halos; (iv) PR accretion with DM halos.

5.1 The impact of the accretion model

Replacing the BHL model with the PR model does not significantly affect the CMB constraint, as long as the effect of DM mini-halos is ignored. This is a highly non-trivial result, given the significant difference of the functional dependence of the accretion rate on the relative BH speed. The reason for this consistency is the accidental cancellation of two competing effects. On the one hand, at recombination and shortly after, the PR model provides a *larger* accretion rate, see Figure 1. At these redshifts, the relative baryon-DM velocity tends towards values that correspond to the high-velocity regime in the PR accretion rate. In this

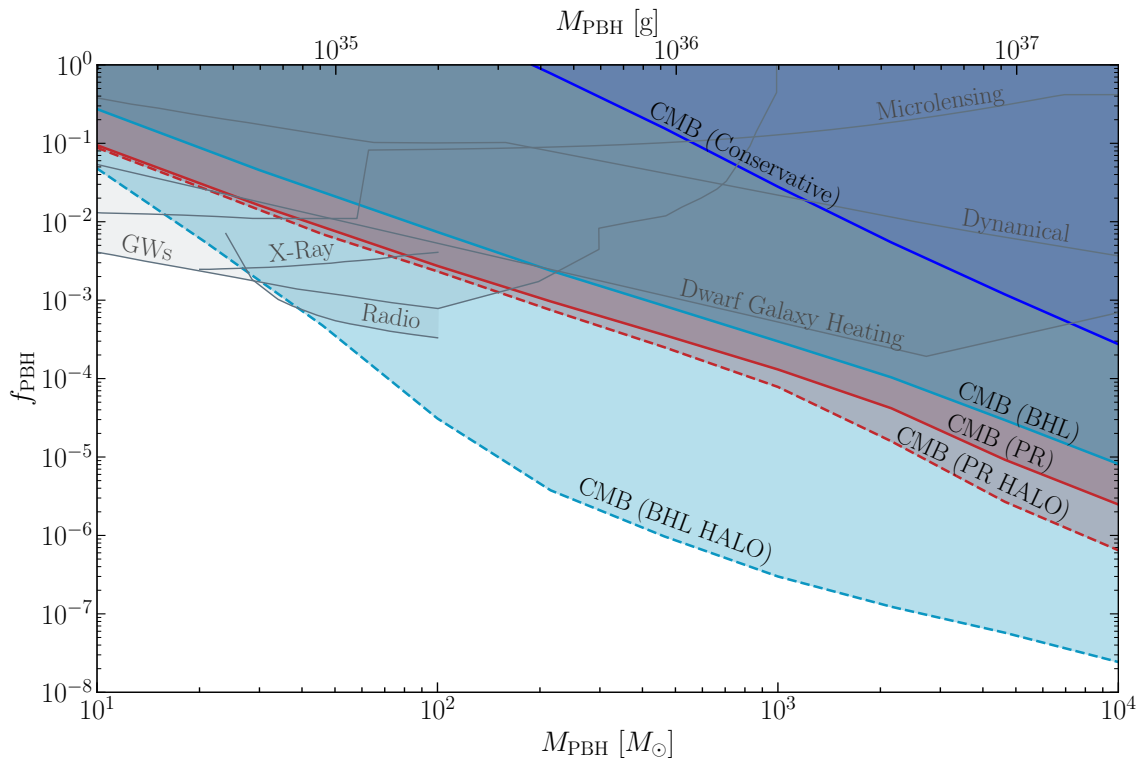


Figure 6: Constraints at the 95% probability from the posterior of f_{PBH} – which describes the cosmological abundance of PBHs as a fraction of the DM abundance, assuming a monochromatic PBH mass function – obtained within different accretion recipes and for a selected range of PBH masses. In light blue is the bound assuming BHL accretion with a disk geometry and with either DM halos included (dashed, “CMB (BHL HALO)”) or not included (solid, “CMB (BHL)”). In red is the bound assuming PR accretion with a disk geometry and with either DM halos included (dashed, “CMB (PR HALO)”) or not included (solid, “CMB (PR)”). The dark blue line (“CMB (Conservative)”) shows the CMB accretion bound following the spherical accretion recipe of §6.4. The most stringent and relevant PBH bounds in this mass regime are also shown from gravitational waves [74, 75], Radio and X-Ray [76], Microlensing [77–79], Dynamical [80, 81], and Dwarf Galaxy Heating [82]. We make use of [83] for plotting.

regime, as discussed in §2.3, the PR model predicts accretion rates higher by a factor $\sim \lambda$ than the BHL model. On the other hand, at lower redshifts, the velocity decreases and the PR model enters its intermediate regime, where a shock front is formed and the accretion rate becomes very strongly suppressed. The two effects partially compensate, resulting in a difference of a factor [2.5 – 3] between the two bounds. In conclusion, while one may have naively expected a *weakening* of the bound in the PR case as a consequence of the low-velocity suppression of the accretion rate, the aforementioned cancellation actually slightly moves the bound in the opposite direction, making it more stringent.

Varying the value of the sound speed $c_{s,\text{in}}$ can change the ratio between the PR and BHL accretion rates, as is shown in Figure 1. We analyze the impact of this parameter on the PR bound in section §6.1.

5.2 The impact of DM mini-halos

We obtain the CMB bound including DM mini-halos following the prescription described in §3. As discussed there, this consists in computing an enhanced accretion rate expressed in terms of an effective Bondi radius. This radius defines an effective cross section for the accretion process and is obtained comparing the total potential of the BH plus the DM halo to the effective velocity v_{eff} , which depends on the relative BH-gas velocity and on the gas sound speed. This is computed through Eq. (3.2) and represented in Figure 2.

In the context of the PR model, we assumed and verified a posteriori that the accretion process, including in the presence of DM mini-halos, occurs within the local ionized region around the BH (we assume this region to be around 10^2 times larger than the Bondi radius [47]). Within this region, temperatures are much higher than those of the neutral background medium. Following the PR prescription, we set the sound speed of the ionized gas to a constant value, choosing as a reference $c_{\text{s,in}} = 23$ km/s, which corresponds to a temperature of a few tens of thousands of Kelvin. As already discussed in §3, the high value of the local effective velocity that follows prevents the DM mini-halos from significantly contributing to the accretion rate. This is reflected in the behavior of the constraint, which is barely affected by the inclusion of the DM mini-halos. We find an effect of at most a factor of a few at the largest PBH masses considered.

To obtain the bound in the BHL case, we perform an analysis similar to that of [14].⁵ The evolution with redshift of the effective velocity is determined by the linear velocity, which evolves as in Eq. (2.3) and by the background value of the sound speed c_{s} , which is computed by CLASS taking into account the energy injection from PBHs.

Comparing the dashed lines in Figure 6, we observe that, when the effect of DM mini-halos around PBHs is taken into account, the constraint obtained with the PR model is weaker by up to 3 orders of magnitude than the constraint obtained with the BHL model. As discussed in §3, the analysis carried out in the BHL case is likely to be overestimating the impact of DM mini-halos. The local increase in the gas sound speed due to the accretion process should be taken into account to correctly quantify the contribution of mini-halos to the accretion rate.

6 Results: Assessment of the astrophysical uncertainties

We now aim to assess the most relevant astrophysical uncertainties that affect the CMB constraints, namely: *i*) the value of the ionized sound speed *ii*) the evaluation of the radiative output associated with the accretion disk; *iii*) the evaluation of the energy deposited in the IGM. Using a PBH mass of $10^3 M_{\odot}$ as the reference value, we compute the posterior distribution function associated with the fractional abundance of PBHs, f_{PBH} , for different values of the parameters which control the aforementioned uncertainties. We show these posteriors in Figure 7, shading the regions excluded at 95% probability.

6.1 Ionized sound speed

The value of $c_{\text{s,in}}$, which characterizes the temperature of the ionized region, alters the functional form of \dot{M} in the PR model, varying the position of the peak as a function of the PBH speed (see Figure 8). The temperature of the ionized medium is in principle fully

⁵Ref. [14] used results of their simulations to describe the DM profile; we rely on the analytical model. They comment in their paper that the difference in the bound is a factor ~ 2 .

determined by the balance between heating and cooling of the material within the ionized region. However, in the PR model it is treated as a constant free parameter. This should be regarded as an approximation for two reasons. Firstly, the temperature of the ionized medium is expected to present a gradient with distance from the BH. Secondly, the amount of heating is tied to the energy injected by the BH and is hence expected to a) be a function of the parameters that enter the accretion rate itself (PBH mass, gas density), b) depend on the efficiency of the energy emission processes. We consider that this approximation is validated by the ability of the PR model to reproduce the results of the simulations, in which the dependencies and feedback mentioned above are taken into account.

Using the results presented in [84] as a guide, we consider as our benchmark $c_{s,\text{in}} = 23$ km/s. In [84], simulations were performed for different values of the density and temperature of the ambient gas, as well as the BH mass. The results show that the temperature profile of the ionized gas presents order one variations with these parameters, being determined in particular by the product of gas density and BH mass.⁶ Moreover, the BH luminosity was assumed to scale with the accretion rate with a slightly different recipe from the one we use here, leading to a luminosity that is lower by around a factor of ten.

Given the uncertainty associated with this kind of modeling, it is interesting to explore how our result are affected by the value of $c_{s,\text{in}}$. We show our posteriors on f_{PBH} for different choices of this parameter in the top row of Figure 7. We see that the impact on the posterior distribution function associated with the fractional abundance of PBHs, f_{PBH} , can be in principle quite significant: an increase (decrease) of $c_{s,\text{in}}$ by a factor of 3 weakens (strengthens) the bound by two orders of magnitude.

Given the sensitivity of the bounds to the precise choice of $c_{s,\text{in}}$, additional simulations of the radiative feedback from the accretion onto PBHs adapted to the specific cosmological settings are needed.

6.2 Radiative efficiency

As explained in §4.1, the efficiency of the energy transfer to the leptonic component of the accretion flow, usually called δ , is a key parameter. In fact, it controls the radiative efficiency, and ultimately the amount of gravitational binding energy that is not advected into the PBH but ultimately radiated and absorbed in the surrounding medium.

We display in the mid-row of Figure 7 the impact of this parameter, δ , on the constraint on the fractional abundance of PBHs. Adopting the three reference values extracted from [22], the position of the upper limit is shifted by roughly an order of magnitude. However, given the discussion in §4.1 about the physical interpretation of the parameter, it turns out that, despite a preferential transfer of energy to the ions, the electron plasma can also be heated up by a variety of kinetic processes in the context of MHD turbulence. Therefore, the very low values of these parameters that would in principle allow for a significant weakening of the bound do not appear to be realistic, and we can conclude that the result is reasonably robust with respect to the uncertainties associated with radiative cooling.

6.3 Energy deposition function

The impact of the different methods that we consider for the computation of the energy deposition into the medium is shown in the bottom row of Figure 7. The different recipes

⁶See Figure 5 of Ref. [84]

described in §4.2 produce result that differ by a factor of a few, and the overall uncertainty on the final result is slightly less than an order of magnitude.

We note that the choice of the *extrapolated* transfer functions decreases the value of the energy deposition functions, thus reducing the deposited energy, and weakening the bound. This is due to $0 < T(z', z, \omega) < 1$ in the extrapolated region ($\omega < 5$ keV) of Eq. (4.6).

6.4 A conservative cosmological bound

It is important to point out that all the results discussed so far rely on the hypothesis that an *accretion disk* is formed. We now relax this assumption, and assess how the bound weakens in the case of *spherical accretion* within our framework. Given all the previous discussion on the uncertainties, we aim at computing the *most conservative upper limit* within the physical setup considered in this work. In order to do so, we adopt the following setup. As far as the accretion rate and radiative efficiency are concerned, we refer to the formalism presented in [13] for the case of spherical accretion. That paper presents an analytical computation of both the fudge factor λ that appears in the BHL formula and the radiative efficiency ϵ . The recipe is valid *in the absence of an accretion disk* and is characterized by a much lower emission of photons with respect to the disk case. The λ factor takes into account the presence of the Compton drag and Compton cooling by CMB photons, and the radiative efficiency formula captures the physics of free-free emission, the main process at work within these assumptions. Regarding the energy deposition, we also adopt the most conservative prescription, i.e. the *extrapolated transfer function*, which, as shown above, determines the weakest upper limit.

Motivated by the results discussed in §3 and §5, we make the conservative choice to entirely neglect the effect of the DM mini-halos on the accretion rate. We show the resulting constraint as a solid dark blue line in Figure 6. In this very conservative setup, the bound is weakened by more than an order of magnitude, but still quite strong, especially for large masses. The most conservative upper limit is still the most stringent available bound towards $M = 10^4 M_\odot$. Beyond this threshold, our examination of the CMB, treating PBHs as a DM fluid component, would likely break down.

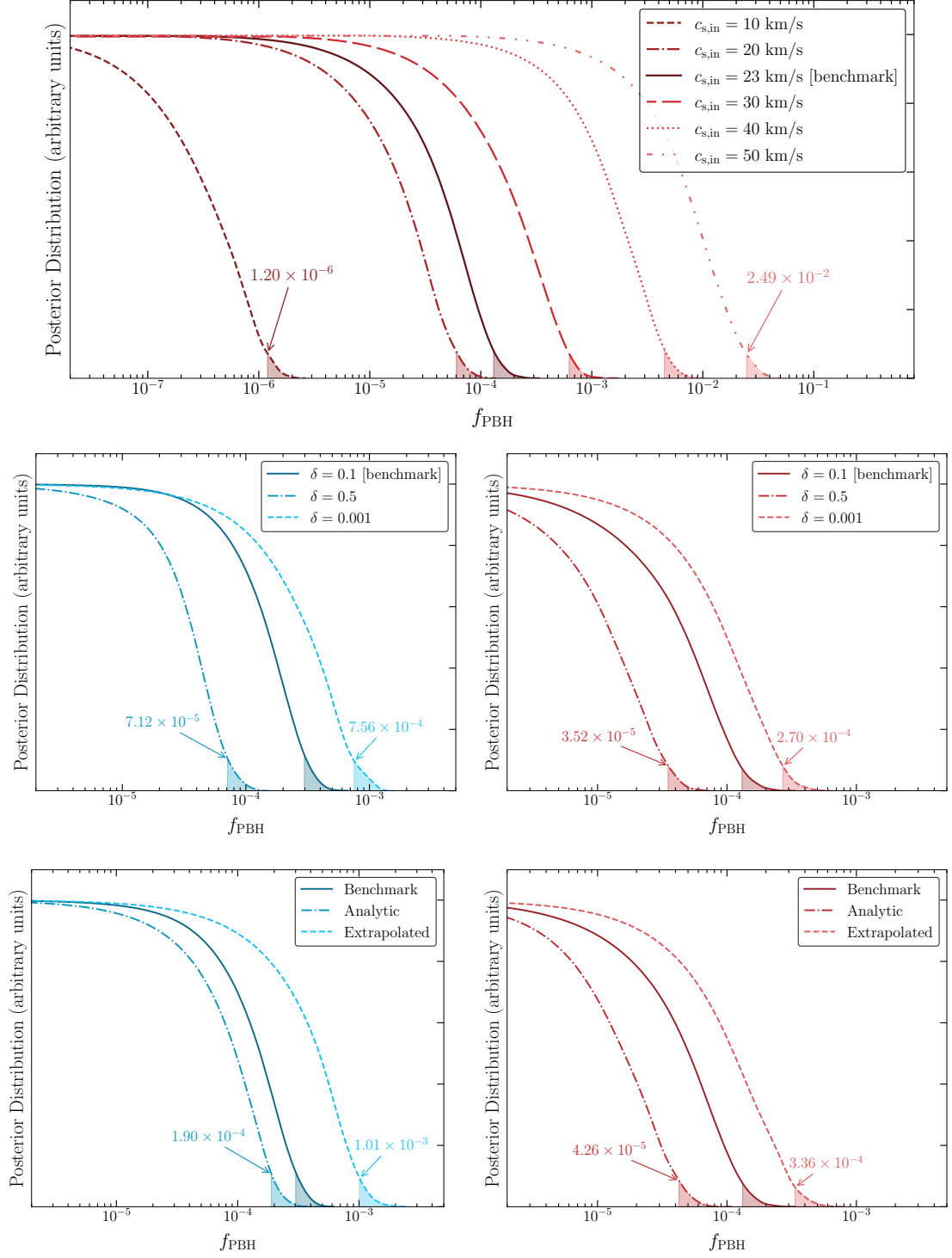


Figure 7: Marginalized posterior distributions of f_{PBH} (in arbitrary units) showing the effect of each ingredient in the accretion recipe entering in the CMB bound for a benchmark PBH mass of $10^3 M_{\odot}$. The 95% probability region is shaded for each posterior, and the bound is labelled for the two extrema for each panel. In particular, the top panel shows the effect of the ionized sound speed in the PR model. The middle panel shows the effect of varying δ in an ADAF accretion scenario for the BHL (left) and the PR (right) models (see Table 1, and Eq. (4.4) for details on δ). The bottom panel shows the effect of different energy deposition function treatments for BHL (left) and PR (right).

7 Discussion and conclusions

In this work, we have critically reviewed the ingredients at the core of the cosmological constraint on accreting PBHs. This bound stems from the energy injected by the PBHs into the inter-galactic medium during the dark ages, which affects both the optical depth and the visibility function of CMB photons. Such a bound depends a priori on a variety of astrophysical details. We discussed the key role of the modeling of baryonic accretion as well as the contribution from DM mini-halos when the fraction of DM that is in the form of PBHs, f_{PBH} , satisfies $f_{\text{PBH}} \ll 1$, inspecting for the first time the interplay between the two, see [Figure 2](#) and [Figure 3](#). We have derived the CMB bound on a handful of realistic physics cases, paying attention once again to the interplay of baryonic accretion with the formation of DM mini-halos, see [Figure 6](#).

When the effect of DM mini-halos around PBHs is taken into account, *the constraint obtained within the PR model is weaker by up to 3 orders of magnitude than that obtained within the BHL model*. Moreover, our analysis suggests that the BHL estimate is likely to be overestimating the impact of DM mini-halos, as the local increase of the sound speed has not been taken into account. The PR model provides a simple way to account for this increase. In a model-independent fashion, we can conclude that *the local increase in temperature and ionization fraction, which we expect to be induced by the accretion process, drastically reduces the impact of DM mini halos on the accretion rate and hence on the CMB bound on PBHs*.

We have then systematically investigated the impact of what we believe to be the key astrophysical ingredients entering in the cosmological analysis of massive PBHs, quantifying their effect on f_{PBH} for a reference PBH mass of $10^3 M_{\odot}$ in [Figure 7](#). Finally, on the basis of our exploration of the main astrophysical phenomena at stake, we singled out a conservative bound on massive PBHs from the CMB, highlighted in dark blue in [Figure 6](#).

It seems natural for us to conclude that despite the multitude of astrophysical uncertainties and the technicalities of the numerical analysis involved, the CMB can easily rule out massive PBHs as light as $10 M_{\odot}$ as DM candidates. However, it remains true that a very conservative approach to the physics of the bound can robustly exclude $f_{\text{PBH}} > 0.1$ only for PBHs of mass equal or greater than $6 \times 10^2 M_{\odot}$ at 95% probability.

In light of these conclusions, we note the following:

- The relative velocity between DM and baryons plays a crucial role in our treatment. Therefore, one may wonder how to quantify the uncertainty on this parameter. The first issue is that the linear approximation adopted in this work inevitably breaks down at late time when virialized halos start to form. The second issue is that it may not apply at the small scales relevant for accretion. These issues are particularly complex and require dedicated simulations to be properly addressed. The first issue does not seem to impact the result presented here, since the effect on the CMB is dominated by the energy injection that happens at $z > 200$, prior to the formation of large virialized halos with significant velocity dispersions. Regarding the second issue, the authors of [\[85, 86\]](#) have shown that the presence of PBHs and their clustering may imply an enhancement of the power spectrum at small scales, but it is unclear whether these early-forming structures can acquire a significant baryon content at early times. The results of the simulations seem to suggest that the non-linear small-scale corrections to the relative DM-baryon velocity associated with this effect are subdominant with respect to the corrections at large scales, and thus the impact on the CMB bound

is considered negligible in these works. Further studies are certainly needed in this direction to better clarify and quantify these issues.

- The (possibly combined) impact of a broad mass function and/or a significant initial clustering on the results presented here might be non-trivial. The effect of a broader mass function, for instance a log-normal centered around a specific mass value, has been extensively discussed in the literature, and remapping procedures were devised in order to properly remap the bound [26]. The upper limits do not show a significant weakening when these procedures are applied. It is more complicated to assess whether less trivial mass functions featuring multiple peaks at relevant mass scales possibly associated with modifications of the equation of state at some critical events in the early universe thermal history [87–89] can evade the bound. In particular, the combination of such peculiar shapes for the mass function and a significant initial clustering of the PBHs may in principle alter all the current upper limits (see discussions on initial clustering and related phenomenology in some specific formation models, e.g. in [90–92]).

Whether the aforementioned points may effectively change any of the conclusions drawn from the outcome reported in Figure 6 poses an interesting question. A convincing answer to that likely requires dedicated N-body simulations, which go beyond the scope of the present study.

Acknowledgments

D.G. acknowledges support from the project “Theoretical Astroparticle Physics (TAsP)” funded by INFN. D.A. acknowledges support from the Generalitat Valenciana under the grant CIGRIS/2021/054. M.V. acknowledges support from the project “Theoretical Particle Physics and Cosmology (TPPC)” funded by INFN. R.E. acknowledges support from the US Department of Energy (DOE) under Grant DE-SC0009854, from the Heising-Simons Foundation under Grant No. 79921, from the Simons Foundation under the Simons Investigator in Physics Award 623940, and from the Binational Science Foundation under Grant No. 2020220. G.S. was supported in part by the DOE under Grant DE-SC0009854 and the Simons Foundation under the Simons Investigator in Physics Award 623940. D.G., F.S, and M.V. are grateful to the organizers of the workshop “Future Perspectives on Primordial Black Holes” for fruitful and vibrant discussions on PBHs. F.S acknowledges support from the ANR project GaDaMa (ANR-18-CE31-0006). We are particularly grateful to the authors of Ref.s [1, 2] for very fruitful exchange and/or communication during all the stages of the present work.

A Details on the Park-Ricotti model

The PR accretion rate is given by

$$\dot{M}_{\text{PR}} = 4\pi \frac{(GM)^2 \rho_{\text{in}}}{(v_{\text{in}}^2 + c_{\text{s,in}}^2)^{3/2}}, \quad (\text{A.1})$$

where v_{in} , ρ_{in} , and $c_{\text{s,in}}$ are, respectively, the values of the BH velocity, gas density, and sound speed within the ionized region. Three regimes exist (see [20, 93] for more details), depending

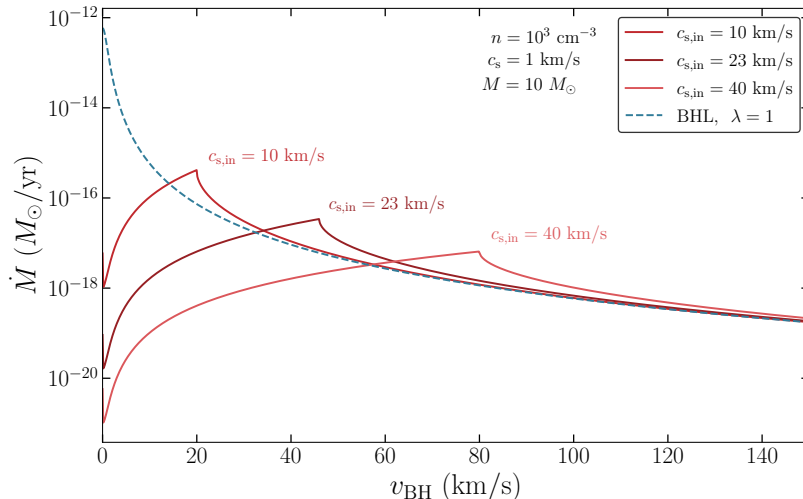


Figure 8: The PR accretion rate as a function of the BH-gas relative speed, for different values of the sound speed of the ionized gas. The BHL rate is shown for comparison.

on the value of the black hole speed with respect to the gas:

- high-velocity regime: $v_{\text{rel}} \geq v_{\text{R}} \approx 2c_{\text{s,in}}$

$$\begin{cases} \rho_{\text{in}} = \rho \frac{v_{\text{rel}}^2 + c_{\text{s}}^2 - \sqrt{\Delta}}{2c_{\text{s,in}}^2}, \\ v_{\text{in}} = \frac{\rho}{\rho_{\text{in}}} v_{\text{rel}} \end{cases} \quad (\text{A.2})$$

- low-velocity regime: $v_{\text{rel}} \leq v_{\text{D}} \approx c_{\text{s}}^2/(2c_{\text{s,in}})$

$$\begin{cases} \rho_{\text{in}} = \rho \frac{v_{\text{rel}}^2 + c_{\text{s}}^2 + \sqrt{\Delta}}{2c_{\text{s,in}}^2}, \\ v_{\text{in}} = \frac{\rho}{\rho_{\text{in}}} v_{\text{rel}} \end{cases} \quad (\text{A.3})$$

- intermediate velocity regime (a shock front is formed): $v_{\text{D}} < v_{\text{rel}} < v_{\text{R}}$

$$\begin{cases} \rho_{\text{in}} = \rho \frac{v_{\text{rel}}^2 + c_{\text{s}}^2}{2c_{\text{s,in}}^2}, \\ v_{\text{in}} = c_{\text{s,in}} \end{cases} \quad (\text{A.4})$$

$\Omega_b \times 10^2$	$\Omega_c \times 10^2$	h	$\ln(10^{10} A_s)$	n_s	z_{reio}	f_{PBH}
$\mathcal{U}(0.5, 4)$	$\mathcal{U}(0.1, 36)$	$\mathcal{U}(0.6, 0.8)$	$\mathcal{U}(1.61, 3.91)$	$\mathcal{U}(0.8, 1.2)$	$\mathcal{U}(4, 10)$	$\mathcal{U}(0, 1)$

Table 3: Cosmological parameters varied in this work and their respective priors. \mathcal{U} denotes a uniform distribution between the specified `min` and `max` values.

where Δ is given by

$$\Delta = \sqrt{(v_{\text{rel}}^2 + c_s^2)^2 - 4v_{\text{rel}}^2 c_{s,\text{in}}^2} \quad (\text{A.5})$$

and $v_{\text{R}}, v_{\text{D}}$, with $v_{\text{R}} > v_{\text{D}}$ are the values for which $\Delta = 0$.

B Details on the numerical analysis

In this work, we made use of the Bayesian code `Cobaya` [59, 60] for our statistical analysis, adopting the `CosmoMC` algorithm [94] as the Monte Carlo Markov Chain (MCMC) sampler. We also took advantage of `getdist` [95] for processing the resulting chains. Following the Planck collaboration [61], we sampled our Λ CDM cosmological parameters with a bounded uniform flat prior, as reported in Table 3.

We used the same Λ CDM parameters as the Planck collaboration, with the exception of sampling directly over the Hubble constant h instead of the angular acoustic scale θ_* , and over the redshift of reionization z_{reio} instead of the optical depth to reionization τ_{reio} . This choice avoided a *shooting* problem encountered in `CLASS` when computing the reionization history.⁷ We verified that Λ CDM parameters are mostly unchanged when PBHs are included, and when using different accretion models, as shown in Figure 9. With this in mind, we provided covariance matrices of the proposal posterior distribution functions (pdfs) for all known cosmological and nuisance parameters, which we derived from running a long Λ CDM run using all our cosmological likelihoods (see the list and references in §4.3). This method allows for more efficient sampling, when extending to the 7-dimensional Λ CDM + f_{PBH} parameter space, and we manually entered an estimate for the reference and proposal for f_{PBH} .⁸

C Comparison to previous works

Considerable effort was made to conduct a consistency check with previous works [1, 2]. In this appendix, we compare our benchmark model to those presented in [1, 2], and we comment on our attempt to replicate their results exactly. As shown in Figure 10 our benchmark results are within approximately an order of magnitude to those in the literature. There are, however, many important differences that distinguish our recipes. Roughly speaking, discrepancies can be attributed to our different treatments of the energy deposition functions, PBH relative velocities, recombination code and `CLASS` versions, and our use of more recent and different likelihoods. We provide a more detailed description of these discrepancies below.

⁷See the documentation of `CLASS` for more details [58].

⁸The value of the proposal defines a proposal pdf which is a Gaussian mixed with an exponential in random directions, which is less sensitive to poor initial-width estimates [96–98].

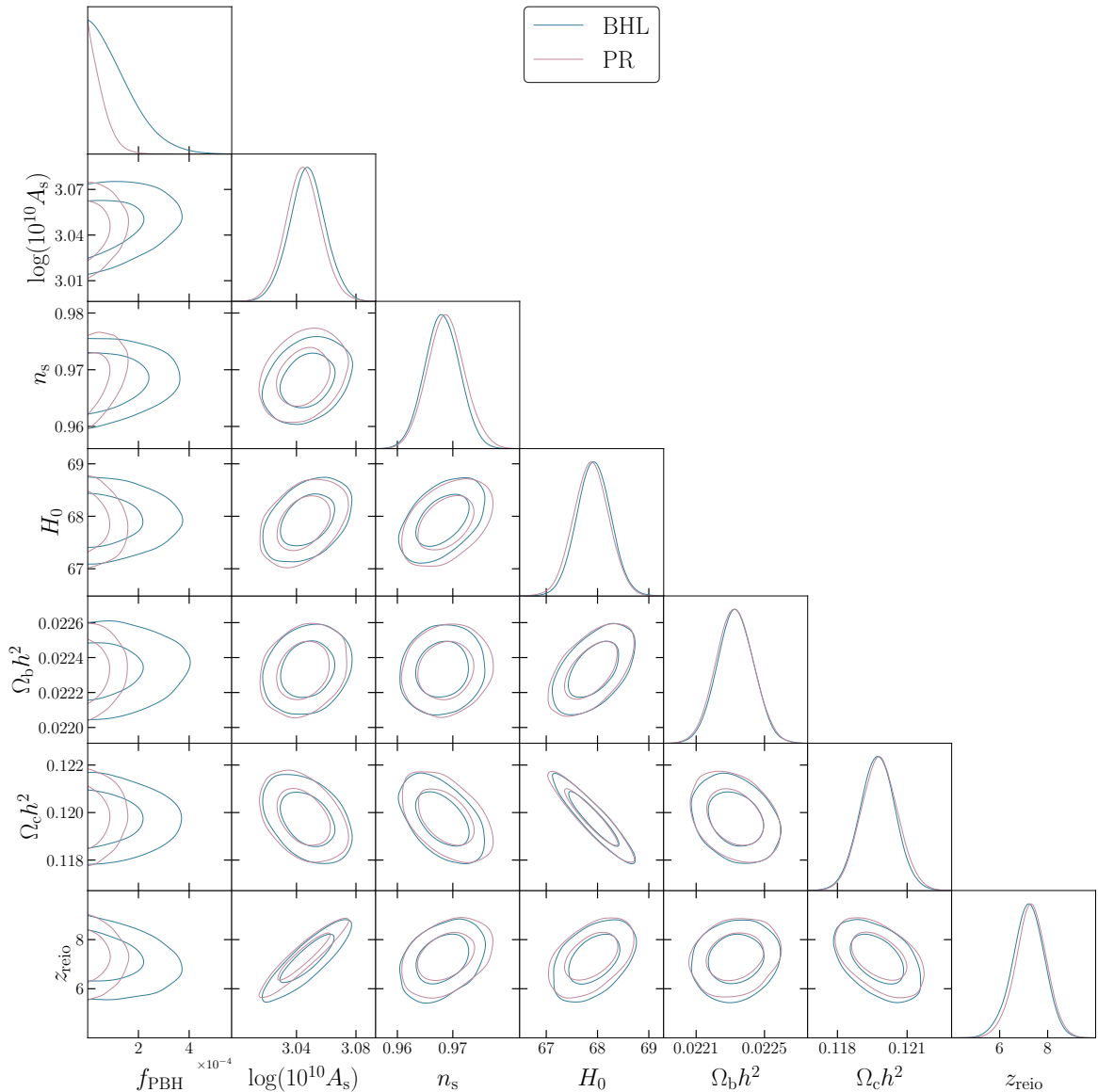


Figure 9: A triangle plot comparing the posteriors at 68% and 95% at $M = 10^3 M_\odot$ for BHL and PR.

C.1 Comparison to Ref. [1]

In this section, FLC2023 refers to the PR model implemented in [1]. Although the underlying PR accretion rate implemented in our work does not differ from FLC2023,⁹ there is an important difference in the technique used to average over the PBH velocity distribution. As previously shown in [13], incorporating PBH velocities in the Bondi formula is done through the transformation,

$$\dot{M}_B \sim \frac{1}{c_s^3} \quad \rightarrow \quad \dot{M}_{\text{BHL}} \sim \frac{1}{(c_s^2 + v_{\text{PBH}}^2)^{3/2}}. \quad (\text{C.1})$$

⁹We use the same sound speed in the ionized region $c_{s,\text{in}} = 23$ km/s.

Since the speed of sound is given by Eq. (2.2), the above transformation is equivalent to

$$\dot{M}_B \sim \frac{1}{c_s^3(X_e, T)} \quad \rightarrow \quad \dot{M}_{\text{BHL}} \sim \frac{1}{c_s^3\left(X_e, T + \frac{m_p v_{\text{PBH}}^2}{\gamma(1+X_e)}\right)}. \quad (\text{C.2})$$

In effect, PBH velocities can be accounted for simply by averaging over the speed of sound in the Bondi model. FLC2023 sets the explicit velocity dependence in the PR model to the root-mean-square (rms) value and then performs this transformation to the speed of sound, integrating it over a Maxwell-Boltzmann distribution.

However, this temperature transformation is only applicable to the Bondi case. In the PR model, the velocity dependence is ‘built-in’, so we simply average over a Maxwell-Boltzmann distribution centered at the baryon-DM relative speed given in Eq. (2.3).

Additionally, FLC2023 uses a radiative efficiency model as described by

$$\epsilon = \epsilon_0 \min\left(1, \frac{\dot{M}_{\text{PBH}}}{L_{\text{Edd}}}\right), \quad (\text{C.3})$$

where ϵ_0 is a scale factor that they fix to 0.1. In particular, this different functional form means that the luminosity scales as $L \propto \dot{M}^2 \propto M_{\text{PBH}}^4$ below the Eddington limit. This is contrary to our use of the ADAF formalism as presented in §4.1, where $L \propto \dot{M}^{1+a} \propto \dot{M}_{\text{PBH}}^{2(1+a)}$, where a takes a piecewise form depending on the accretion rate (but primarily takes the value $a = 0.59$). This different scaling of the luminosity with M , is one of the factors leading to a different slope in Figure 10. Furthermore, [1] uses a different energy deposition treatment, where (referring to the second equality in Eq. (4.5)) they choose to use the $f_{\text{eff}}(z)$ function derived analytically by [13], with the repartition functions χ_c computed by [53]. There are also differences in the likelihoods, the sampling technique,¹⁰ and the statistical treatment of the posterior in the computation of the bound.

In addition to the comparison shown in Figure 10, we attempted to directly reproduce the results of [1]. We thank [1] for sharing their version of CLASS with us. For the MCMC sampler, [1] used MontePython [99, 100] to infer their cosmological parameters, but we checked that the result remains unchanged irrespective of the sampler by comparing directly between the results of Cobaya and MontePython. Using their exact version of CLASS, as well as a version we modified to replicate their results, we consistently found a result differing by roughly a factor of 4 across the entire mass range. We attribute this difference to their log sampling and a different statistical treatment of their posterior.

C.2 Comparison to Ref. [2]

In this section, PSCCK2017 refers to the BHL disk accretion model implemented in [2]. Despite using the same BHL model and disk accretion geometry, there are a number of important differences that cause our bounds to differ from their bounds.

The primary reason for this discrepancy is the treatment of PBH velocities. PSCCK2017 uses an approximated effective velocity formula,

$$\dot{M}_{\text{BHL}} \sim \frac{1}{v_{\text{eff}}^3} \quad \text{where} \quad v_{\text{eff}} \equiv \left\langle \frac{1}{(c_s^2 + v_{\text{rel}}^2)^3} \right\rangle^{-1/6} \simeq \sqrt{c_s \sqrt{\langle v_{\text{rel}}^2 \rangle}}. \quad (\text{C.4})$$

¹⁰FLC2023 uses a log-spaced prior on f_{PBH} , compared to our uniform linear prior.

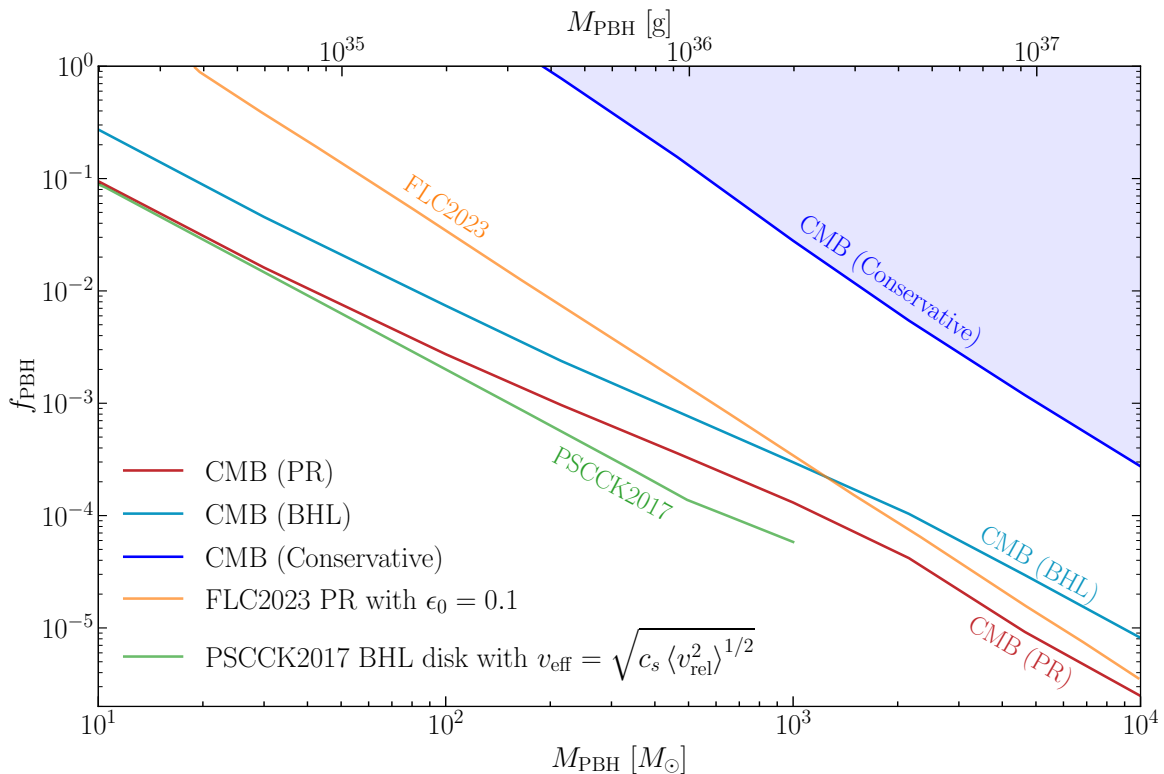


Figure 10: Bounds at 95% probability on the abundance of a monochromatic distribution of PBHs, with a comparison to previous works. In light blue, we show our bound assuming BHL accretion with disk geometry without DM mini-halos, in red, we show the bound assuming PR accretion with disk geometry without DM mini-halos, and in dark blue, we show the conservative bound assuming spherical accretion [equivalent to those shown in Figure 6]. In orange, we show the bound computed by [1] (FLC2023) using the PR model and reference value of $\epsilon_0 = 0.1$. In green, we show the bound computed by [2] (PSCCK2017), using the BHL model with disk accretion, and $v_{\text{eff}} = \sqrt{c_{s,\infty} \langle v_{\text{rel}}^2 \rangle}^{1/2}$. There are a number of differences between these recipes, which we describe in detail in Appendix C.

This formula implicitly assumes that the total luminosity is quadratic with the accretion rate. Although this is true for a linear efficiency, in the ADAF efficiency model, the scaling is not quadratic and a proper averaging over a Maxwell-Boltzmann distribution is needed.¹¹ Additionally, the constraint in PSCCK2017 was calculated using different energy deposition functions, as described in §4.2. In our approach, we cut the transfer functions at 5 keV whereas PSCCK2017 extrapolates down to 100 eV. Moreover, the functional form of the luminosity spectrum used by PSCCK2017 could not be exactly determined. Consequently, we were unable to replicate Fig. 2 in [2]. Finally, these results relied on Planck 2015 likelihoods, whereas we use the more recent Planck 2018 likelihoods as well as other cosmological data sets. Considerable efforts were made to compare directly to this work by implementing to the best of our ability the recipe used by [2]. Unfortunately, an exact replication of their results was not possible due to some uncertainties regarding their recipe, but for our best attempt, our bounds differed only by an overall $\mathcal{O}(1)$ factor.

¹¹This is expanded on in detail in [101], where the nuance of this calculation is described in their Eq. (3.6).

References

- [1] G. Facchinetti, M. Lucca and S. Clesse, *Relaxing cmb bounds on primordial black holes: the role of ionization fronts*, *Physical Review D* **107** (Feb., 2022) 043537, [[2212.07969](#)].
- [2] V. Poulin, P. D. Serpico, F. Calore, S. Clesse and K. Kohri, *CMB bounds on disk-accreting massive Primordial Black Holes*, *Physical Review D* **96** (Oct., 2017) 083524.
- [3] P. J. E. Peebles, S. Seager and W. Hu, *Delayed recombination*, *Astrophys. J. Lett.* **539** (2000) L1–L4, [[astro-ph/0004389](#)].
- [4] E. Pierpaoli, *Decaying particles and the reionization history of the universe*, *Physical Review Letters* **92** (Jan., 2004) 031301.
- [5] X.-L. Chen and M. Kamionkowski, *Particle decays during the cosmic dark ages*, *Phys. Rev. D* **70** (2004) 043502, [[astro-ph/0310473](#)].
- [6] N. Padmanabhan and D. P. Finkbeiner, *Detecting dark matter annihilation with cmb polarization: Signatures and experimental prospects*, *Physical Review D* **72** (July, 2005) 023508.
- [7] L. Zhang, X. Chen, Y.-A. Lei and Z.-g. Si, *Impacts of dark matter particle annihilation on recombination and the anisotropies of the cosmic microwave background*, *Physical Review D* **74** (Nov., 2006) 103519.
- [8] L. Zhang, X. Chen, M. Kamionkowski, Z.-g. Si and Z. Zheng, *Constraints on radiative dark-matter decay from the cosmic microwave background*, *Physical Review D* **76** (Sept., 2007) 061301.
- [9] B. J. Carr, *Pregalactic black hole accretion and the thermal history of the universe*, *MNRAS* **194** (Feb., 1981) 639–668.
- [10] M. Ricotti, *Bondi accretion in the early universe*, *Astrophys. J.* **662** (2007) 53–61, [[0706.0864](#)].
- [11] L. Chen, Q.-G. Huang and K. Wang, *Constraint on the abundance of primordial black holes in dark matter from Planck data*, *JCAP* **12** (2016) 044, [[1608.02174](#)].
- [12] B. Horowitz, *Revisiting Primordial Black Holes Constraints from Ionization History*, [1612.07264](#).
- [13] Y. Ali-Haïmoud and M. Kamionkowski, *Cosmic microwave background limits on accreting primordial black holes*, *Physical Review D* **95** (feb, 2017) .
- [14] P. D. Serpico, V. Poulin, D. Inman and K. Kohri, *Cosmic microwave background bounds on primordial black holes including dark matter halo accretion*, *Phys. Rev. Res.* **2** (2020) 023204, [[2002.10771](#)].
- [15] F. Hoyle and R. A. Lyttleton, *The effect of interstellar matter on climatic variation*, *Mathematical Proceedings of the Cambridge Philosophical Society* **35** (July, 1939) 405–415.
- [16] H. Bondi, *On spherically symmetrical accretion*, *MNRAS* **112** (Jan., 1952) 195.
- [17] H. Bondi, *On spherically symmetrical accretion*, *Monthly Notices of the Royal Astronomical Society* **112** (Jan., 1952) 195.
- [18] K. Park and M. Ricotti, *Accretion onto Black Holes from Large Scales Regulated by Radiative Feedback. I. Parametric Study for Spherically Symmetric Accretion*, *The Astrophysical Journal* **739** (Aug., 2011) 2.
- [19] K. Park and M. Ricotti, *Accretion onto Black Holes from Large Scales Regulated by Radiative Feedback. II. Growth Rate and Duty Cycle*, *The Astrophysical Journal* **747** (Mar., 2012) 9.

- [20] K. Park and M. Ricotti, *Accretion onto Black Holes from Large Scales Regulated by Radiative Feedback. III. Enhanced Luminosity of Intermediate Mass Black Holes Moving at Supersonic Speeds*, *The Astrophysical Journal* **767** (Apr., 2013) 163.
- [21] K. J. Mack, J. P. Ostriker and M. Ricotti, *Growth of structure seeded by primordial black holes*, *Astrophys. J.* **665** (2007) 1277–1287, [[astro-ph/0608642](#)].
- [22] F.-G. Xie and F. Yuan, *Radiative efficiency of hot accretion flows*, *Monthly Notices of the Royal Astronomical Society* **427** (nov, 2012) 1580–1586.
- [23] T. R. Slatyer, *Energy Injection And Absorption In The Cosmic Dark Ages*, *Phys. Rev. D* **87** (2013) 123513, [[1211.0283](#)].
- [24] T. R. Slatyer, *Indirect Dark Matter Signatures in the Cosmic Dark Ages II. Ionization, Heating and Photon Production from Arbitrary Energy Injections*, *Physical Review D* **93** (Jan., 2016) 023521.
- [25] D. P. Finkbeiner, S. Galli, T. Lin and T. R. Slatyer, *Searching for dark matter in the cmb: A compact parametrization of energy injection from new physics*, *Physical Review D* **85** (Feb., 2012) .
- [26] N. Bellomo, J. L. Bernal, A. Raccanelli and L. Verde, *Primordial black holes as dark matter: converting constraints from monochromatic to extended mass distributions*, *Journal of Cosmology and Astroparticle Physics* **2018** (Jan., 2018) 004–004.
- [27] F. Kühnel and K. Freese, *Constraints on primordial black holes with extended mass functions*, *Physical Review D* **95** (Apr., 2017) .
- [28] B. Carr, M. Raidal, T. Tenkanen, V. Vaskonen and H. Veermäe, *Primordial black hole constraints for extended mass functions*, *Physical Review D* **96** (July, 2017) .
- [29] D. Tseliakhovich and C. Hirata, *Relative velocity of dark matter and baryonic fluids and the formation of the first structures*, *Phys.Rev.D82:083520,2010* **82** (Oct., 2010) 083520, [[1005.2416](#)].
- [30] C. Dvorkin, K. Blum and M. Kamionkowski, *Constraining dark matter-baryon scattering with linear cosmology*, *Phys.Rev.D89:023519,2014* **89** (Jan., 2013) 023519, [[1311.2937](#)].
- [31] R. Perna, R. Narayan, G. Rybicki, L. Stella and A. Treves, *Bondi accretion and the problem of the missing isolated neutron stars*, *The Astrophysical Journal* **594** (sep, 2003) 936.
- [32] R. Fender, T. Maccarone and I. Heywood, *The closest black holes*, *Mon. Not. Roy. Astron. Soc.* **430** (2013) 1538, [[1301.1341](#)].
- [33] S. Pellegrini, *Nuclear accretion in galaxies of the local universe: Clues from chandra observations*, *The Astrophysical Journal* **624** (may, 2005) 155.
- [34] Q. D. Wang et al., *Dissecting X-ray-emitting Gas around the Center of our Galaxy*, *Science* **341** (2013) 981, [[1307.5845](#)].
- [35] M. Ricotti, J. P. Ostriker and K. J. Mack, *Effect of Primordial Black Holes on the Cosmic Microwave Background and Cosmological Parameter Estimates*, *Astrophys. J.* **680** (June, 2008) 829–845, [[0709.0524](#)].
- [36] K. Park, *Accretion onto Black Holes from Large Scales Regulated by Radiative Feedback*. Phd thesis, University of Maryland, 2012.
- [37] V. Berezhinsky, V. Dokuchaev and Y. Eroshenko, *Formation and internal structure of superdense dark matter clumps and ultracompact minihaloes*, *Journal of Cosmology and Astroparticle Physics* **2013** (Nov., 2013) 059–059.
- [38] M. S. Delos, A. L. Erickcek, A. P. Bailey and M. A. Alvarez, *Are ultracompact minihalos really ultracompact?*, *Phys. Rev. D* **97** (2018) 041303, [[1712.05421](#)].

- [39] J. Adamek, C. T. Byrnes, M. Gosenca and S. Hotchkiss, *WIMPs and stellar-mass primordial black holes are incompatible*, [1901.08528](#).
- [40] M. Boudaud, T. Lacroix, M. Stref, J. Lavalley and P. Salati, *In-depth analysis of the clustering of dark matter particles around primordial black holes. Part I. Density profiles*, *JCAP* **08** (2021) 053, [[2106.07480](#)].
- [41] J. Adamek, C. T. Byrnes, M. Gosenca and S. Hotchkiss, *WIMPs and stellar-mass primordial black holes are incompatible*, *Phys. Rev. D* **100** (July, 2019) 023506, [[1901.08528](#)].
- [42] E. Bertschinger, *Self-similar secondary infall and accretion in an Einstein-de Sitter universe*, *ApJS* **58** (May, 1985) 39–65.
- [43] B. Carr, F. Kühnel and L. Visinelli, *Black holes and wimps: all or nothing or something else*, *Monthly Notices of the Royal Astronomical Society* **506** (July, 2021) 3648–3661.
- [44] Y. N. Eroshenko, *Dark matter density spikes around primordial black holes*, *Astronomy Letters* **42** (June, 2016) 347–356.
- [45] M. Boudaud, T. Lacroix, M. Stref, J. Lavalley and P. Salati, *In-depth analysis of the clustering of dark matter particles around primordial black holes. part i. density profiles*, *Journal of Cosmology and Astroparticle Physics* **2021** (Aug., 2021) 053.
- [46] K. Park, M. Ricotti, P. Natarajan, T. Bogdanović and J. H. Wise, *Bulge-driven Fueling of Seed Black Holes*, *ApJ* **818** (Feb., 2016) 184, [[1512.03434](#)].
- [47] K. Sugimura and M. Ricotti, *Structure and instability of the ionization fronts around moving black holes*, *MNRAS* **495** (July, 2020) 2966–2978, [[2003.05625](#)].
- [48] S. L. Shapiro and A. P. Lightman, *Black holes in X-ray binaries: marginal existence and rotation reversals of accretion disks.*, *ApJ* **204** (Mar., 1976) 555–560.
- [49] N. I. Shakura and R. A. Sunyaev, *Black holes in binary systems. Observational appearance.*, *A&A* **24** (Jan., 1973) 337–355.
- [50] L. Arzamasskiy, M. W. Kunz, B. D. G. Chandran and E. Quataert, *Hybrid-kinetic simulations of ion heating in alfvénic turbulence*, *The Astrophysical Journal* **879** (jul, 2019) 53.
- [51] S. S. Cerri, L. Arzamasskiy and M. W. Kunz, *On Stochastic Heating and Its Phase-space Signatures in Low-beta Kinetic Turbulence*, *ApJ* **916** (Aug., 2021) 120, [[2102.09654](#)].
- [52] V. Zhdankin, D. A. Uzdensky, G. R. Werner and M. C. Begelman, *Electron and Ion Energization in Relativistic Plasma Turbulence*, *Phys. Rev. Lett.* **122** (Feb., 2019) 055101, [[1809.01966](#)].
- [53] S. Galli, T. R. Slatyer, M. Valdes and F. Iocco, *Systematic uncertainties in constraining dark matter annihilation from the cosmic microwave background*, *Physical Review D* **88** (Sept., 2013) 063502, [[1306.0563](#)].
- [54] P. Stöcker, M. Krämer, J. Lesgourgues and V. Poulin, *Exotic energy injection with ExoCLASS: Application to the Higgs portal model and evaporating black holes*, *Journal of Cosmology and Astroparticle Physics* **2018** (Mar., 2018) 018–018.
- [55] H. Liu, G. W. Ridgway and T. R. Slatyer, *Darkhistory: A code package for calculating modified cosmic ionization and thermal histories with dark matter and other exotic energy injections*, *Phys. Rev. D* **101**, 023530 (2020) **101** (Jan., 2019) 023530, [[1904.09296](#)].
- [56] F. Capozzi, R. Z. Ferreira, L. Lopez-Honorez and O. Mena, *Cmb and lyman- α constraints on dark matter decays to photons*, *Journal of Cosmology and Astroparticle Physics* **2023** (June, 2023) 060, [[2303.07426](#)].
- [57] W. Hu, N. Sugiyama and J. Silk, *The Physics of microwave background anisotropies*, *Nature* **386** (1997) 37–43, [[astro-ph/9604166](#)].

- [58] D. Blas, J. Lesgourgues and T. Tram, *The Cosmic Linear Anisotropy Solving System (CLASS) II: Approximation schemes*, *Journal of Cosmology and Astroparticle Physics* **2011** (July, 2011) 034–034.
- [59] J. Torrado and A. Lewis, *Cobaya: Code for bayesian analysis of hierarchical physical models*, *JCAP 05 (2021) 057* **2021** (May, 2020) 057, [2005.05290].
- [60] J. Torrado and A. Lewis, “Cobaya: Bayesian analysis in cosmology.” Astrophysics Source Code Library, record ascl:1910.019, Oct., 2019.
- [61] P. Collaboration, *Planck 2018 results. VI. Cosmological parameters*, *Astronomy & Astrophysics* **641** (Sept., 2020) A6.
- [62] F. Beutler, C. Blake, M. Colless, D. H. Jones, L. Staveley-Smith, L. Campbell et al., *The 6dF Galaxy Survey: Baryon Acoustic Oscillations and the Local Hubble Constant*, *Monthly Notices of the Royal Astronomical Society* **416** (Oct., 2011) 3017–3032.
- [63] A. J. Ross, L. Samushia, C. Howlett, W. J. Percival, A. Burden and M. Manera, *The Clustering of the SDSS DR7 Main Galaxy Sample I: A 4 per cent Distance Measure at $z=0.15$* , *Monthly Notices of the Royal Astronomical Society* **449** (May, 2015) 835–847.
- [64] S. Alam, M. Ata, S. Bailey, F. Beutler, D. Bizyaev, J. A. Blazek et al., *The clustering of galaxies in the completed SDSS-III Baryon Oscillation Spectroscopic Survey: cosmological analysis of the DR12 galaxy sample*, *Monthly Notices of the Royal Astronomical Society* **470** (Sept., 2017) 2617–2652.
- [65] eBOSS Collaboration, S. Alam, M. Aubert, S. Avila, C. Balland, J. E. Bautista et al., *The Completed SDSS-IV extended Baryon Oscillation Spectroscopic Survey: Cosmological Implications from two Decades of Spectroscopic Surveys at the Apache Point observatory*, *Physical Review D* **103** (Apr., 2021) 083533.
- [66] L. Balkenhol, D. Dutcher, A. S. Mancini, A. Doussot, K. Benabed, S. Galli et al., *A Measurement of the CMB Temperature Power Spectrum and Constraints on Cosmology from the SPT-3G 2018 TT/TE/EE Data Set*, *Physical Review D* **108** (July, 2023) 023510.
- [67] S. Aiola, E. Calabrese, L. Maurin, S. Naess, B. L. Schmitt, M. H. Abitbol et al., *The Atacama Cosmology Telescope: DR4 Maps and Cosmological Parameters*, *Journal of Cosmology and Astroparticle Physics* **2020** (Dec., 2020) 047–047.
- [68] S. K. Choi, M. Hasselfield, S.-P. P. Ho, B. Koopman, M. Lungu, M. H. Abitbol et al., *The Atacama Cosmology Telescope: a measurement of the Cosmic Microwave Background power spectra at 98 and 150 GHz*, *Journal of Cosmology and Astroparticle Physics* **2020** (Dec., 2020) 045–045.
- [69] M. S. Madhavacheril, F. J. Qu, B. D. Sherwin, N. MacCrann, Y. Li, I. Abril-Cabezas et al., *The Atacama Cosmology Telescope: DR6 Gravitational Lensing Map and Cosmological Parameters*, Apr., 2023.
- [70] F. J. Qu, B. D. Sherwin, M. S. Madhavacheril, D. Han, K. T. Crowley, I. Abril-Cabezas et al., *The Atacama Cosmology Telescope: A Measurement of the DR6 CMB Lensing Power Spectrum and its Implications for Structure Growth*, Apr., 2023.
- [71] J. Carron, M. Mirmelstein and A. Lewis, *CMB lensing from Planck PR4 maps*, *Journal of Cosmology and Astroparticle Physics* **2022** (Sept., 2022) 039.
- [72] A. Gelman and D. B. Rubin, *Inference from Iterative Simulation Using Multiple Sequences*, *Statistical Science* **7** (Nov., 1992) .
- [73] R. Kumar, C. Carroll, A. Hartikainen and O. Martin, *Arviz a unified library for exploratory analysis of bayesian models in python*, *Journal of Open Source Software* **4** (Jan., 2019) 1143.

- [74] B. J. Kavanagh, D. Gaggero and G. Bertone, *Black holes' dark dress: On the merger rate of a subdominant population of primordial black holes*, *Phys. Rev. D* **98**, 023536 (2018) **98** (July, 2018) 023536, [[1805.09034](#)].
- [75] Z.-C. Chen and Q.-G. Huang, *Distinguishing primordial black holes from astrophysical black holes by einstein telescope and cosmic explorer*, *Journal of Cosmology and Astroparticle Physics* **2020** (Aug., 2019) 039–039, [[1904.02396](#)].
- [76] J. Manshanden, D. Gaggero, G. Bertone, R. M. T. Connors and M. Ricotti, *Multi-wavelength astronomical searches for primordial black holes*, *Journal of Cosmology and Astroparticle Physics* **2019** (June, 2018) 026–026, [[1812.07967](#)].
- [77] M. Oguri, J. M. Diego, N. Kaiser, P. L. Kelly and T. Broadhurst, *Understanding caustic crossings in giant arcs: characteristic scales, event rates, and constraints on compact dark matter*, *Phys. Rev. D* **97**, 023518 (2018) **97** (Jan., 2018) 023518, [[1710.00148](#)].
- [78] T. Blaineau, M. Moniez, C. Afonso, J. N. Albert, R. Ansari, E. Aubourg et al., *New limits from microlensing on galactic black holes in the mass range $10m_{\odot} < m < 1000m_{\odot}$* , *A&A* **664**, A106 (2022) **664** (Aug., 2022) A106, [[2202.13819](#)].
- [79] A. Esteban-Gutiérrez, E. Mediavilla, J. Jiménez-Vicente and J. A. Muñoz, *Constraints on the abundance of pbhs from x-ray quasar microlensing observations: Substellar to planetary mass range*, [2307.07473](#).
- [80] M. A. Monroy-Rodríguez and C. Allen, *The end of the macho era- revisited: new limits on macho masses from halo wide binaries*, *The Astrophysical Journal* **790** (July, 2014) 159, [[1406.5169](#)].
- [81] T. D. Brandt, *Constraints on macho dark matter from compact stellar systems in ultra-faint dwarf galaxies*, *The Astrophysical Journal Letters* **824** (June, 2016) L31, [[1605.03665](#)].
- [82] P. Lu, V. Takhistov, G. B. Gelmini, K. Hayashi, Y. Inoue and A. Kusenko, *Constraining primordial black holes with dwarf galaxy heating*, *Astrophys.J.Lett.* **908** (2021) **2**, L23 **908** (Feb., 2020) L23, [[2007.02213](#)].
- [83] B. J. Kavanagh, *bradkav/pbhbounds: Release version*, 2019. 10.5281/ZENODO.3538999.
- [84] K. Sugimura and M. Ricotti, *Structure and Instability of the Ionization Fronts around Moving Black Holes*, *Mon. Not. Roy. Astron. Soc.* **495** (2020) 2966–2978, [[2003.05625](#)].
- [85] G. Hütsi, M. Raidal and H. Veermäe, *Small-scale structure of primordial black hole dark matter and its implications for accretion*, *Phys. Rev. D* **100** (2019) 083016, [[1907.06533](#)].
- [86] D. Inman and Y. Ali-Haïmoud, *Early structure formation in primordial black hole cosmologies*, *Phys. Rev. D* **100** (2019) 083528, [[1907.08129](#)].
- [87] B. Carr, S. Clesse, J. García-Bellido and F. Kühnel, *Cosmic conundra explained by thermal history and primordial black holes*, *Phys. Dark Univ.* **31** (2021) 100755, [[1906.08217](#)].
- [88] J. C. Niemeyer and K. Jedamzik, *Near-critical gravitational collapse and the initial mass function of primordial black holes*, *Phys. Rev. Lett.* **80** (1998) 5481–5484, [[astro-ph/9709072](#)].
- [89] G. Franciolini, I. Musco, P. Pani and A. Urbano, *From inflation to black hole mergers and back again: Gravitational-wave data-driven constraints on inflationary scenarios with a first-principle model of primordial black holes across the QCD epoch*, *Phys. Rev. D* **106** (2022) 123526, [[2209.05959](#)].
- [90] J. R. Chisholm, *Clustering of primordial black holes: basic results*, *Phys. Rev. D* **73** (2006) 083504, [[astro-ph/0509141](#)].
- [91] G. Ballesteros, P. D. Serpico and M. Taoso, *On the merger rate of primordial black holes: effects of nearest neighbours distribution and clustering*, *JCAP* **10** (2018) 043, [[1807.02084](#)].

- [92] S. Clesse and J. García-Bellido, *The clustering of massive Primordial Black Holes as Dark Matter: measuring their mass distribution with Advanced LIGO*, *Phys. Dark Univ.* **15** (2017) 142–147, [[1603.05234](#)].
- [93] F. Scarcella, *Black Hole Phenomenology and Dark Matter Searches*. Phd thesis, 11, 2023. [2311.11975](#).
- [94] A. Lewis, *Efficient sampling of fast and slow cosmological parameters*, *Phys. Rev. D* **87** (2013) 103529, [[1304.4473](#)].
- [95] A. Lewis, *GetDist: a Python package for analysing Monte Carlo samples*, [1910.13970](#).
- [96] R. M. Neal, *Taking bigger metropolis steps by dragging fast variables*, [math/0502099](#).
- [97] A. Lewis and S. Bridle, *Cosmological parameters from cmb and other data: a monte-carlo approach*, *Phys.Rev.D66:103511,2002* **66** (Nov., 2002) 103511, [[astro-ph/0205436](#)].
- [98] A. Lewis, *Efficient sampling of fast and slow cosmological parameters*, *Phys. Rev. D* **87**, 103529 (2013) **87** (May, 2013) 103529, [[1304.4473](#)].
- [99] B. Audren, J. Lesgourgues, K. Benabed and S. Prunet, *Conservative Constraints on Early Cosmology: an illustration of the Monte Python cosmological parameter inference code*, *JCAP* **1302** (2013) 001, [[1210.7183](#)].
- [100] T. Brinckmann and J. Lesgourgues, *MontePython 3: boosted MCMC sampler and other features*, [1804.07261](#).
- [101] O. Mena, S. Palomares-Ruiz, P. Villanueva-Domingo and S. J. Witte, *Constraining the primordial black hole abundance with 21-cm cosmology*, *Physical Review D* **100** (Aug., 2019) .